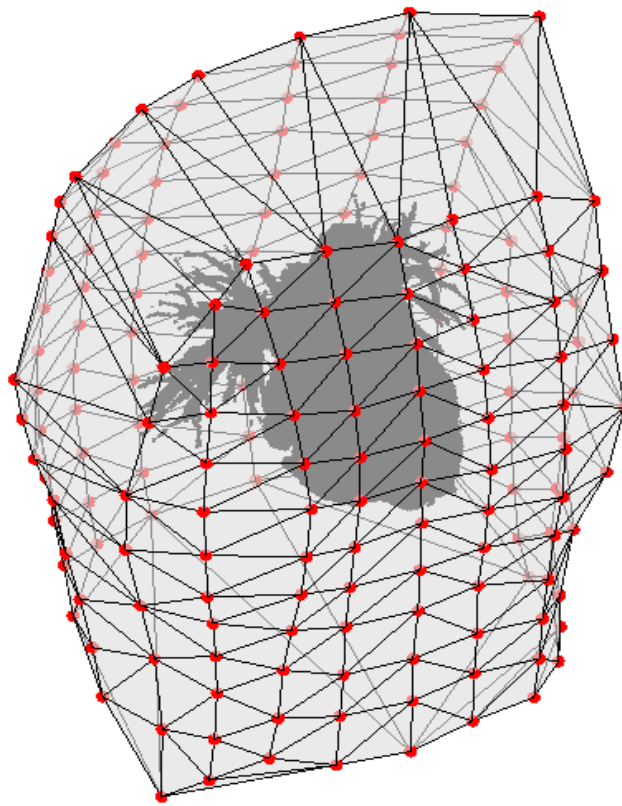


Non-invasive electrocardiographic imaging in patients with idiopathic ventricular fibrillation:

Number and placement of body-surface electrodes for the assessment of epicardial repolarization

Master thesis



D.J.M. Schipaanboord

Medical Sensing & Stimulation, Technical Medicine, University of Twente
Department of Cardiology, UMC Utrecht



UMC Utrecht

UNIVERSITY OF TWENTE.

Graduation committee

Chairman:	Prof. C.H. Slump, PhD
Technical supervisor:	B.E. Westerhof, PhD
Medical supervisor:	R.J. Hassink, MD, PhD
Process supervisor:	N.S. Cramer Bornemann, MSc
Daily (additional) supervisors:	S.A. Groeneveld, MD L.J. Blom, MD, PhD
External member:	E. Mos-Oppersma, PhD

Abstract

Introduction: The diagnosis idiopathic ventricular fibrillation (IVF) is established in sudden cardiac arrest patients in whom the underlying cause is unidentifiable. It is hypothesized that the cause may lie in repolarization abnormalities which cannot yet be found with current diagnostics. Non-invasive electrocardiographic imaging (ECGI) can be used to gain insight in cardiac electrophysiology. With ECGI, the electrical potentials at the epicardium are reconstructed from its projected body-surface potentials. However, no consensus exists on the necessary number and distribution of body-surface electrodes for high quality ECGI in IVF patients. Therefore, the objective of this study was to assess how the body-surface potentials measurement should be performed for high quality ECGI regarding the assessment of regional repolarization differences.

Methods: Data of ten ECGI measurements, performed on IVF patients with a 184-electrodes set-up, were used. A simulated inter-system comparison was performed (i.e. smaller electrode set-ups were selected from the 184-electrodes set-ups, without changing other ECGI aspects). First, the ECGI quality of a 64-electrodes set-up, 62-electrodes set-up and the standard 9-electrodes set-up were investigated in comparison to the 184-electrodes set-up. In total, 50 sinus rhythm (SR) beats and ten ventricular extra systoles (VES) were reconstructed for each set-up. Second, the necessary number and positioning of the body-surface electrodes was investigated by removal and addition of electrodes to the 64-electrodes set-up. Ten SR beats and VES were reconstructed for each adjusted set-up. The reconstructions were compared based on several outcome measures, including the T-wave correlation. Furthermore, electrodes which seemed of less value for the reconstruction were removed to find the limit of necessary electrodes.

Results: High median T-wave correlation coefficients (CC_T (Q1 - Q3)) between the 184-electrodes set-up and the 64-electrodes set-up ($CC_{T,SR}$: 0.98 (0.92 - 0.99), $CC_{T,VES}$: 0.98 (0.91 - 0.99)) and 62-electrodes set-up ($CC_{T,SR}$: 0.96 (0.88 - 0.99), $CC_{T,VES}$: 0.97 (0.87 - 0.99)) were found. In contrast to the standard 9-electrodes set-up ($CC_{T,SR}$: 0.85 (0.14 - 0.97), $CC_{T,VES}$: 0.83 (0.11 - 0.96)). The results suggested that the 64-electrodes set-up and 62-electrodes set-up are sufficient and that the standard 9-electrodes set-up is insufficient. A lower limit of number of electrodes was found around 45 electrodes. The left anterior quadrant of the thorax and inferior torso area proved of value for the inverse reconstruction, whereas the right lateral side and posterior side of the thorax proved of less value. This study increases our understanding of the effect of electrode number and placement in ECGI.

List of abbreviations

AT	Activation time
AUC	Area under the curve
BSP	Body-surface potential
BSPM	Body-surface potential mapping
CT	Computed tomography
ECG	Electrocardiogram
ECGI	Electrocardiographic imaging
EDL	Equivalent double layer
EGM	Electrogram
ICD	Implantable cardioverter-defibrillator
IVF	Idiopathic ventricular fibrillation
LV	Left ventricle
MRI	Magnetic resonance imaging
MUMC+	Maastricht University Medical Centre+
NOI	Node of interest
PPS	Pericardial potential source
RT	Recovery time
RV	Right ventricle
SCA	Sudden cardiac arrest
SNR	Signal-to-noise ratio
SR	Sinus rhythm
UMC	University Medical Centres
UMCU	University Medical Centre Utrecht
VES	Ventricular extra systole(s)
VF	Ventricular fibrillation

Contents

1. Introduction	11
2. Background	13
2.1. Idiopathic ventricular fibrillation.....	13
2.2. Ventricular repolarization.....	13
2.3. Electrocardiographic imaging.....	14
2.3.1. Fundamental principle of ECGI.....	14
2.3.2. Validation & clinical application	15
2.3.3. Model assumptions and drawbacks.....	16
3. Methods	17
3.1. Current set-ups.....	17
3.1.1. Study design.....	17
3.1.2. Data acquisition	19
3.1.3. Data analysis	19
3.2. Optimal set-up	26
3.2.1. Study design.....	26
3.2.2. Data analysis	26
4. Results	29
4.1. Current set-ups.....	29
4.1.1. T-wave correlation	29
4.1.2. Activation and recovery time	30
4.1.3. Activation and recovery duration.....	31
4.1.4. Repolarization gradients	32
4.1.5. Regional differences	33
4.1.6. Effect of amplitude and noise	39
4.2. Optimal set-up	41
4.2.1. Removal of electrodes.....	41
4.2.2. Addition of electrodes.....	43
4.2.3. Optimal set-up.....	45
5. Discussion	48
5.1. Ground truth	50
5.2. Electrode set-ups.....	50
5.3. Inverse reconstruction.....	51
5.4. Outcome measures.....	52
5.5. Future perspectives	52
6. Conclusion	53
7. References	54

1. Introduction

Sudden cardiac arrest (SCA) is a major health problem worldwide.¹ In Europe, the incidence rate of out-of-hospital cardiac arrest is 84 per 100.000 population per year.² SCA is an unexpected cardiac arrest without obvious extracardiac cause.³ Aetiology can be determined in ~93% of the patients.⁴ Ventricular fibrillation (VF) is the arrhythmia most often recorded during SCA.⁵ Patients, with documentation of VF, in whom the underlying cause is unidentifiable are diagnosed with idiopathic VF (IVF).⁶

Due to the lack of an identifiable substrate, the underlying pathophysiological mechanism of IVF is unknown. The diagnosis is established by exclusion of known cardiac, respiratory, metabolic and toxicological causes.⁶ Concerning therapy for IVF, no apparent pathogenesis can be targeted. The recurrence rate of arrhythmias in IVF patients is high, approximately 31% during 5 years follow-up.⁷ For secondary prevention of SCA, an implantable cardioverter-defibrillator (ICD) is advised.⁶ A recent study investigated ICD therapy and its complications in patients registered in the Dutch national IVF registry. Of all IVF patients ~96% had an ICD implanted, from which 29.5% received shocks. Inappropriate therapy was delivered in 17.5% of all IVF patients with an ICD, and in 14.7% complications were seen.⁸

The absence of a known underlying cause in IVF is unsatisfactory for both patient and physician. Increased understanding can lead to specific diagnoses and additional therapy options. More insight in the pathogenesis of IVF can therefore be of great value. Considering the occurrence of repolarization abnormalities in known arrhythmogenic disorders, it is hypothesized that the cause of VF in IVF patients may lie in repolarization abnormalities that cannot yet be found with current diagnostics.⁹ Steep regional repolarization gradients for instance provide a substrate susceptible for re-entrant tachyarrhythmias.^{10,11} Thus, to gain more insight in the pathogenesis of IVF, assessment of the electrical activity and recovery at the myocardium level is necessary.

Currently used diagnostics to assess cardiac electrophysiology have their limitations. The standard 12-lead electrocardiogram (ECG) lacks the capacity to assess regional de- and repolarization with high resolution. In contrast, catheter-based high-density electro-anatomical mapping during electrophysiology studies can be used to assess the regional electrophysiology with high resolution, but is invasive, time-consuming, expensive, can lead to complications and frequently no electrophysiological abnormalities are found endocardially.¹² An emerging non-invasive technique is electrocardiographic imaging (ECGI).¹³ With ECGI, electrical activity at the myocardium is reconstructed from its projected body-surface potentials (BSPs). This technique can be valuable to increase insight in the cardiac electrophysiology of IVF patients.

The VIGILANCE project focuses on the use of ECGI in patients with IVF.¹⁴ This project is a collaboration between the department of cardiology of the University Medical Centre Utrecht (UMCU), Maastricht University Medical Centre+ (MUMC+) and the Amsterdam University Medical Centres (Amsterdam UMC). For the VIGILANCE project an observationally cohort study has been started, with the objective to noninvasively screen IVF patients for an epicardial electrophysiological substrate and triggers using ECGI, and to evaluate the ECGI mappings for risk stratification.

For ECGI, the ECGs on the body surface are usually measured with tens or even hundreds of electrodes on the torso.^{15,16,17,18} The number and positioning of body-surface electrodes for ECGI are still under debate.¹³ Donnelly et al.¹⁹ suggested that 24-35 electrodes for body-surface potential mapping (BSPM), with their recording site carefully chosen, can accurately determine all ECG information. Hoekema et al.²⁰ recommended that the number of electrodes used for BSPM should be in the order of 64, to pick up the major part of ECG information. Furthermore, the electrodes should be placed non-uniformly on both anterior and posterior chest and with the highest density of electrodes at the left anterior chest.²⁰ As regards ECGI quality, limited research has been done on the minimal number and optimal positioning of body-surface electrodes. In 2015, Cluitmans et al.²¹ evaluated the necessary number of electrodes for ECGI reconstructions of high quality in dogs. They simultaneously measured potentials at the body

surface and the epicardium and investigated the correlation. Different electrode set-ups, consisting of 169, 108, 80, 68, 59, 10, 9 and 3 electrodes, were compared. Their results indicate a reasonably stable reconstruction quality from 169 to 59 electrodes.²¹ However, they did not investigate the effect of the position of the electrodes on the torso. Unfortunately, current studies are not focussed on evaluation of the ECGI quality in patients with IVF. Evaluation on outcome measures focussing on repolarization are therefore necessary. In short, the necessary number and distribution of electrodes sufficient to provide good quality ECGI is not known. Therefore the research question of this study is:

Research question: How to perform the body-surface potentials measurement for high quality ECGI regarding the assessment of regional repolarization differences?

As a first step in answering the research question, it is of interest to know the ECGI quality for currently used body-surface electrode set-ups of the participating hospitals of the VIGILANCE study. The number and positioning of electrodes differ between the participating hospitals of the VIGILANCE study. For instance, in the MUMC+ 184 electrodes are used, while in the UMCU 64 electrodes are used with different distributions on the torso. The Amsterdam UMC does not have a fixed ECGI measurement set-up yet. In published research performed at the Amsterdam UMC, a set-up of 62-electrodes was used for body-surface potential mapping.²² Furthermore, it is interesting to investigate the ECGI quality of the standard 9-electrodes set-up. Currently, there is doubt whether the smaller electrode set-ups (~ 60 electrodes) are suitable for performing qualitative ECGI in patients with IVF. In addition, it is of added value to know whether ECGI outcomes for different electrode set-ups are comparable, so that data can be pooled.

Based on the literature, it is hypothesized that set-ups consisting of more than 59 electrodes provide sufficient ECGI quality.^{19,20,21} Therefore, it is hypothesized that the standard 9-electrodes set-up is insufficient and all set-ups of the participating hospitals in the VIGILANCE study are sufficient for use in ECGI. The MUMC+ set-up consists of a considerably higher number of electrodes in comparison to the other set-ups. Therefore, it is hypothesized that the MUMC+ set-up provides sufficient ECGI quality and can be used as 'ground truth'. Hence, the first sub question of this study is:

Sub question 1: What is the reconstruction accuracy of the UMCU 64-electrodes, Amsterdam UMC 62-electrodes and standard 9-electrodes set-up relative to the MUMC+ 184-electrodes 'ground truth' set-up regarding the assessment of regional repolarization differences?

As a second step in answering the research question, the necessary number and positioning of electrodes for the body-surface potentials measurement is investigated. It is hypothesized that the limit of electrodes necessary for sufficient ECGI quality is below 59 electrodes. However, with decreasing number of electrodes, the electrode placement is increasingly important, where it is hypothesized that it is important to have electrodes both anterior and posterior and a high density of electrodes left anterior of the chest. The second sub question of the study is:

Sub question 2: What is the necessary number and positioning of the body-surface electrodes for high quality ECGI regarding the assessment of regional repolarization differences?

2. Background

2.1. Idiopathic ventricular fibrillation

The prevalence of IVF in the Netherlands is unknown, but was estimated at 1,000 patients in 2018. Remarkably, the IVF population generally consists of young people, with a mean age of 38 years.¹⁴

IVF is a *diagnosis of exclusion*, hence many diagnostic tests must be deployed. Routine testing for IVF usually consists of electrocardiography, blood chemistry, toxicological screening, Holter or telemetry monitoring, echocardiography, chest X-ray, exercise-testing, coronary angiography with or without ventriculography and MRI. Recommended additional tests are: ergonovine and ajmaline provocation. Endomyocardial biopsy, electrophysiological testing and targeted genetic screening based on phenotype are optional additional tests, since their diagnostic value is under debate.²³

The IVF diagnosis is probably overused.⁴ The certainty of IVF depends on the extensiveness of diagnostic testing. Patients are often diagnosed with IVF after limited diagnostic testing.²⁴ Studies showed the importance of follow-up and systematic clinical evaluation in revealing specific diagnoses in patients initially diagnosed with IVF.^{4,24,25,26}

Moreover, several primary arrhythmia disorders have been discovered, which were initially considered IVF. Currently, it is possible to differentiate long QT, catecholaminergic polymorphic ventricular tachycardia, Brugada syndrome, short QT and early repolarization syndrome from IVF.^{6,23} The differentiation is mainly facilitated by the advance in phenotypic and genetic analysis. Some other discoveries, such as the CALM1 and DPP6 mutation, are still not associated with a fitting phenotype. Therefore, it is hypothesized that the aetiology of IVF is heterogeneous.²³

Family members of IVF patients might also have predisposition for sudden cardiac arrests.²⁷ Early recognition of people prone to malignant arrhythmias can be valuable in the prevention of life-threatening events. Unfortunately, the lack of clinical signs in IVF patients leads to difficulties for risk stratification.

2.2. Ventricular repolarization

Ventricular repolarization is represented by the T-wave on the ECG (Figure 1). The T-wave on the BSPs represents repolarization of the entire heart, whereas the T-wave on local electrograms (EGMs) represent local repolarization.^{9,28} In contrast to depolarization, repolarization is relatively slow and the potential differences over larger distances are smaller which provide temporally static potential patterns.^{29,30} The T-wave is mainly influenced by the intrinsic properties of cardiomyocytes (action potential duration).³¹ The ventricular myocardium consist of three cell types: epicardial, endocardial, and M cells. These cells differ in repolarization characteristics.³² For instance, M cells can have their action potentials prolonged disproportionately to epicardial and endocardial cells.³³ In physiological conditions, electronic coupling keeps closely coupled cells in synchrony. The loss of strength of electronic coupling can induce large local repolarization differences.³⁴

Meijborg et al.⁹ investigated normal ventricular repolarization in Langendorff perfused pig hearts. They found the start of ventricular repolarization at the right ventricle (RV). In the left ventricle (LV), repolarization progressed from basal to central. Final repolarization was at the central free walls of the RV and LV. Ventricular repolarization can change if alterations in action potential duration, refractory period or conduction velocity occur.³⁵ For example, large differences in action potential duration over small distances causes steep repolarization gradients. The alterations can be induced by multiple conditions, for instance electrolyte disturbances. Regions with increase in ventricular repolarization heterogeneity are vulnerable for arrhythmias.³⁶ Over the years, ventricular repolarization has gained interest as a potential tool for risk stratification of arrhythmic events.

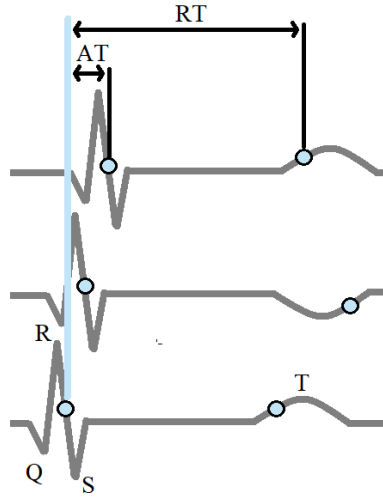


Figure 1: Schematic representation of epicardial EMGs. AT = Activation time. RT = Recovery time.

2.3. Electrocardiographic imaging

2.3.1. Fundamental principle of ECGI

Excitation of the heart generates an electric potential field in the torso volume between the body surface and the epicardium.³⁷ The potentials at the torso (φ_T), which can be measured noninvasively using body-surface electrodes, are a projection of the electrical activity at the myocardium (φ_M). This projection depends on the electromagnetic relation between φ_T and φ_M , which is captured in a transfer matrix (A) (Eq. 1). The transfer matrix contains information of the patient's specific torso-heart geometry and thoracic conductivities.³⁷ The patient-specific-torso-heart geometry can be obtained by CT or MRI.

$$\varphi_T = A\varphi_M \quad (1)$$

Equation 1 describes the so called 'forward model', by which φ_T is computed for a given φ_M (Figure 2). With ECGI, electrical activity at the myocardium (source) is reconstructed from its projected body-surface potentials (output). The reconstruction from known 'output' to unknown 'source' is called the 'inverse model' (Figure 2).¹³ Theoretically, the inverse problem can lead to infinite possible solutions for φ_M .¹⁵ To find solution φ_M which best explains the recorded φ_T , least squares approximation can be performed (Eq. 2).³⁸

$$\min_{\varphi_M} \|A\varphi_M - \varphi_T\|_2^2 \quad (2)$$

However, the inverse model is ill-posed, which means small changes in the measured output, e.g. due to noise, can cause large changes in the solution.³⁹ To apply constraints to the solutions, regularization is required.^{13,39} A well-known regularization method is Tikhonov regularization, with which a stable solution is obtained by setting constraints to the amplitude of the reconstructed φ_M .³⁸

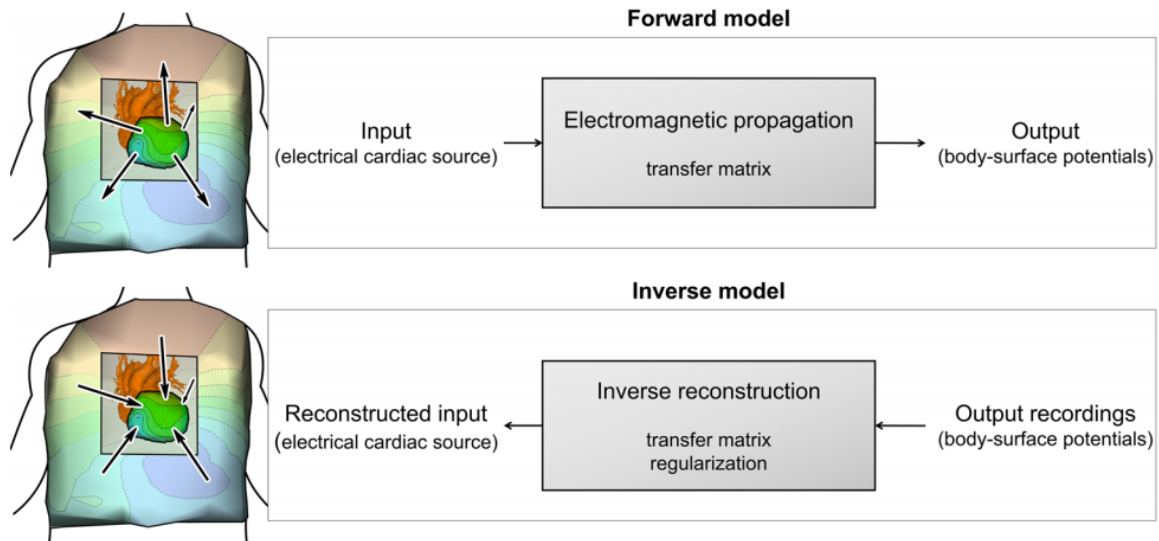


Figure 2: Schematic representation of the ECGI forward and inverse model. Retrieved from ¹³.

For the reconstruction, a model for the cardiac source is necessary. Two often used methods for the cardiac source are: the pericardial potential source (PPS) model and the equivalent double layer (EDL) model. The PPS model is based on a closed surface surrounding the heart as source of the electrical activity. For the EDL model, the cardiac source is defined as an equivalent double layer consisting of the entire surface bounding the myocardium (endocardium and epicardium).⁴⁰

2.3.2. Validation & clinical application

Validation of non-invasive ECGI is performed by torso-tank experiments⁴¹, in animals^{42,43} and in humans¹⁸. Investigations showed that ECGI can capture features of cardiac electrical excitation and can provide extra insights into the electrophysiology of cardiac disorders.^{16,17,18,44,45} Ramanathan et al.³⁰ investigated ventricular repolarization in healthy adults with the use of ECGI. Based on epicardial potential maps, they found positive T-waves anterior (typically in the RV) and negative T-waves at apical and posterior regions of the LV (Figure 3A and 3B). Concerning the RT isochrones maps, shorter RTs were found anterior in comparison to posterior (Figure 3C).

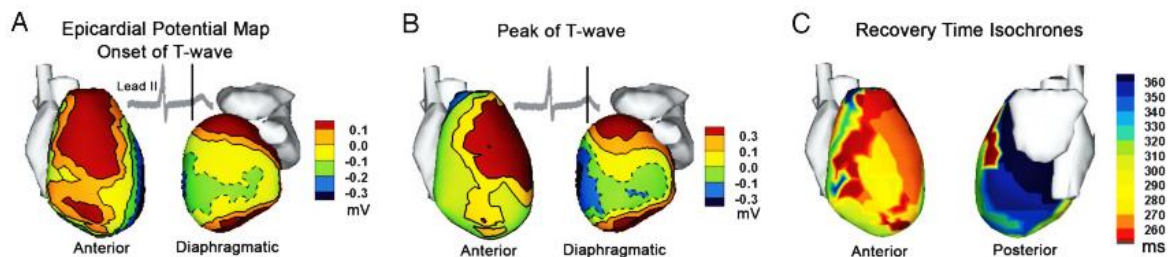


Figure 3: Ventricular repolarization of a healthy adult. A) Anterior and diaphragmatic view of the epicardial potentials map during T-wave onset. B) Anterior and diaphragmatic view of the epicardial potentials map during T-wave peak. C) Anterior and posterior view of epicardial RT isochrones. Adapted from ³⁰.

Focussing on arrhythmogenic disorders, ECGI is able to reveal repolarization abnormalities. In patients with Brugada Syndrome, abnormal repolarization and conduction in the right ventricular outflow tract were identified using ECGI.¹⁶ Furthermore, ECGI revealed steep repolarization gradients in Early

Repolarization Syndrome patients. Vijayakumar et al.¹⁷ found regions with ventricular repolarization delay close to regions with early repolarization, resulting in steep repolarization gradients in long QT syndrome patients with the use of ECGI. In terms of clinical application, ECGI may prove useful in risk screening, diagnosis, guide targeted interventions (e.g. determination of the location of an arrhythmogenic substrate) and follow-up or evaluation of therapy.⁴⁶

2.3.3. Model assumptions and drawbacks

For careful interpretation of the ECGI outcomes it is important to acknowledge the influence of model assumptions and ECGI drawbacks. The inverse model of ECGI consists of the elements: cardiac source representation, body-surface potential measurement, patient-specific transfer matrix and regularization. To illustrate the challenges of ECGI, certain specifications or assumptions for each element will be discussed.

The cardiac source models PPS and EDL yield different reconstruction results. With the PPS model local EGMs at the epicardium can be reconstructed directly. Additional information such as, activation times (ATs) and recovery times (RTs) can be extracted indirectly from these local electrograms.¹³ AT is defined as the time from earliest epicardial activation to the maximal negative slope of the local EGM QRS complex and RT as the time from earliest epicardial activation to the maximal positive slope of the local EGM T-wave (Figure 1).^{16,47} The EDL model is more restricted. Only local ATs and RTs can be reconstructed directly. Due to the sparse representation, however, the EDL model is more robust to noise. In addition, the EDL model provides information of both epicardium and endocardium.¹³

The importance of the body-surface potential measurement is gathering adequate information about the projected electrical activity at the body surface for reconstruction. Therefore, the body-surface potentials should be measured at a sufficient number of positions around the patient's torso. By increasing the number of electrodes, relative to the standard 9 electrodes set-up, higher resolution of the electrical dynamics of the heart can be achieved.^{48,49} However, the question remains at which number of electrodes the resolution approaches its maximum. Furthermore, a high number of electrodes can be redundant and impractical for clinical use. Currently, many different body-surface electrode set-ups are used, while it is not known if all set-ups are providing sufficient ECGI quality for their clinical purposes.

The patient-specific transfer matrix is based on the patient's torso and heart geometry and the conductivity of the tissues in between. The heart surface is based on a geometry extracted from CT or MRI images. The extraction is subject to variations caused by the use of different (manual or automated) extraction techniques and the image quality. The geometry of the torso is obtained from the positions of the electrodes extracted from the CT or MRI, and therefore dependent on the number and distribution of the electrodes. Besides, it is assumed that the geometries are non-moving, while during the BSP measurement the geometries are not static and the conductivity changes.¹³ Regarding the conductivity, the torso volume can be simplified by the assumption of being completely homogenous between heart and torso. Inclusion of inhomogeneities will give a more realistic representation of the torso volume. However, it is more complex which deteriorates applicability of ECGI as a clinical tool. Moreover, it is not yet clear to which extent inclusion of inhomogeneities improves the reconstruction.^{50,51,52}

Finally, the necessary regularization poses challenges. Beside Tikhonov, many other regularization methods exist. All methods have their specific difficulties and have varying performance under different conditions.^{53,54}

3. Methods

This study was performed at the Cardiology department of the UMCU, in collaboration with the Cardiology department of the MUMC+, the Netherlands.

3.1. Current set-ups

3.1.1. Study design

This study investigated the inverse reconstruction accuracy of different body-surface electrode set-ups regarding the assessment of regional repolarization differences. As mentioned in the Introduction section, it is assumed that the MUMC+ set-up provides sufficient ECGI quality and was therefore handled as ‘ground truth’.

Data of ten ECGI measurements performed with the MUMC+ set-up at patients with IVF were used. The MUMC+ set-up consists of ~184 electrodes, which are incorporated in strips consisting of eight or twelve electrodes (Figure 4). To investigate the ECGI quality of some current body-surface electrode set-ups a simulated inter-system comparison was performed. Therefore, the electrodes as placed for the UMCU, Amsterdam UMC and standard 9-electrodes set-up were selected from the electrodes of the MUMC+ set-up (Figure 4). The benefit of the simulated inter-system approach is that the electrode number and position can be changed, while other ECGI aspects remain unchanged.

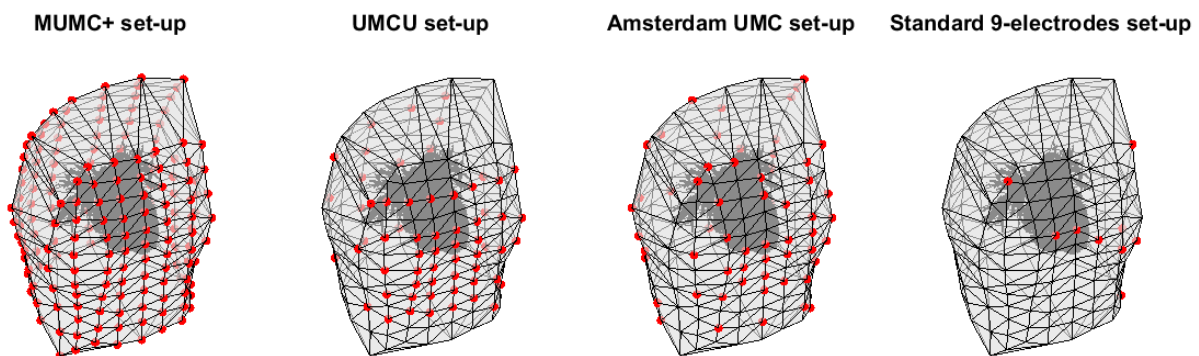


Figure 4: Selection of electrodes of the MUMC+ set-up for the UMCU set-up, Amsterdam UMC set-up and standard 9-electrodes set-up.

Per patient measurement five sinus rhythm (SR) beats at rest were selected. If present also ventricular extra systoles (VES) were selected. ECGI reconstructions were performed for the selected beats for each electrode set-up (Figure 5). To investigate if the ECGI quality of the UMCU, Amsterdam UMC and standard 9-electrodes set-up are comparable to the MUMC+ set-up, the reconstructions of the selected set-ups were compared with the reconstructions of the MUMC+ set-up.

Comparison of reconstructions was performed based on outcome measures focussing on the assessment of regional repolarization differences. Quantitatively outcome measures on a node-to-node basis were used, such as: correlation, absolute AT differences and absolute RT differences. In addition, repolarization gradients were examined. In ECGI, spatial displacement of the reconstruction on the epicardium can take place. Therefore, additional outcome measures, which are not affected by spatial displacement, were necessary. Hence, the difference in total activation and recovery duration were explored. Furthermore, the potential causes for differences were examined by addressing the T-wave amplitude, T-wave polarity and the level of noise in the T-wave segment.

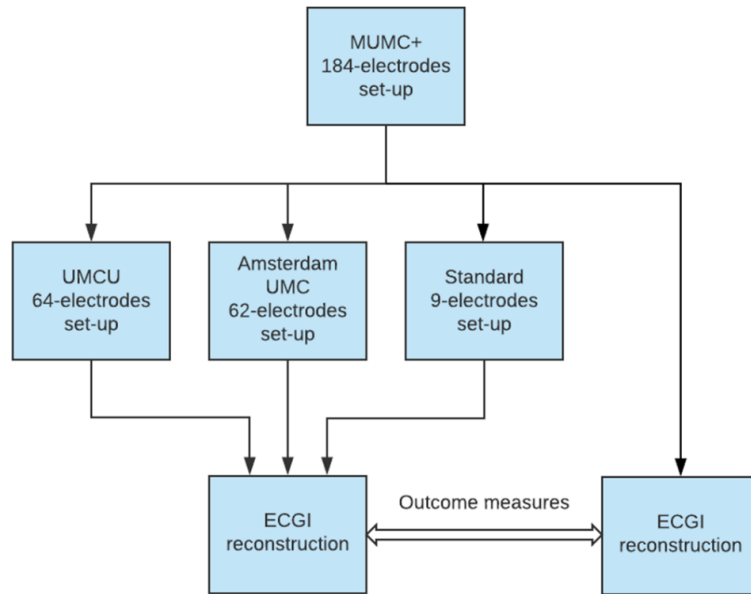


Figure 5: Flowchart of the study design.

3.1.1.1. Electrode set-ups

The MUMC+ electrode set-up is not standardized. In practice, the strips are manually applied with a fairly homogeneous distribution over the thorax based on visual inspection, with a higher density of strips at the anterior side in comparison to the posterior side of the thorax. In contrast to the MUMC+ set-up, the UMCU, Amsterdam UMC and standard 9-electrodes set-up are standardized. The UMCU set-up consists of 64 electrodes (Figure 6), which in practice at the UMCU can be placed separately on the thorax. In this study, the so called Amsterdam UMC set-up is a set-up consisting of 62 electrodes used in published research performed at the Amsterdam UMC (Figure 6).²²

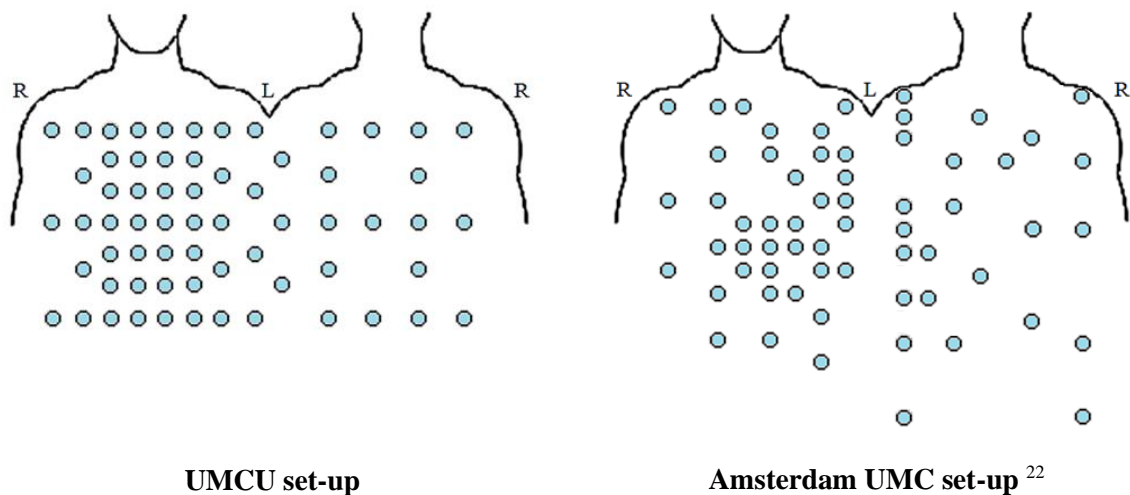


Figure 6: Left) Schematic representation of the UMCU 64-electrodes set-up on the body-surface. Right) Schematic representation of the Amsterdam UMC 62-electrodes set-up on the body-surface.

3.1.2. Data acquisition

For this study, data of ten ECGI measurements were made available by the MUMC+. The BSP measurements were carried out with the MUMC+ set-up and recorded with an acquisition system of BioSemi (BioSemi, Amsterdam, the Netherlands) with a sampling frequency of 2048 Hz. A thoracic low dose CT scan was performed with the electrodes still positioned at the body surface. Thereafter, a CT scan of the diastolic phase of the heart was performed during intravenous injection of iodine contrast medium. The body-surface electrodes, ventricular epicardium and blood pool were manually segmented from the CT-scans by MUMC+ employees with the use of Seg3D (Version 2.2.1, Scientific Computing And Imaging Institute, Utah, USA). For creation of a smooth epicardial mesh of the segmented ventricular epicardium, PreView (Version 2.1.5, Musculoskeletal Research Laboratories, Utah, USA) was used. PreView was also used to reduce the epicardial nodes to ~2000. Nodes are virtual points on the epicardial mesh on which the electrograms are reconstructed.

3.1.3. Data analysis

3.1.3.1. Pre-processing of body-surface potentials

First, the BSPs were inspected in EDFbrowser (Version 1.70, T. van Beelen)⁵⁵. In EDFbrowser sections of ten seconds were selected, which contained the beat(s) of interest. Thereafter, all data were exported to Matlab (R2018b, MathWorks, Natick, MA, USA) for further analysis.

The ECGI procedure consists of a number of pre-processing steps. First, baseline wander was removed from the BSPs by subtracting a linear fit from the original signal. Then, the signal was filtered with a 2 Hz low-pass filter and a first order Savitsky-Golay filter with a window length of maximal two seconds (depending on the signal length). This filtered signal was subtracted from the linearly detrended signal for baseline correction. In addition, the BSPs were filtered with a second order low-pass Butterworth filter with a cut-off frequency of 125 Hz. Furthermore, 50 Hz noise was removed with a first order band-stop Butterworth filter with stopband [48, 52]. Finally, baseline drift was again removed for the selected beat by subtraction of a linear fit.

Not all BSPs are satisfactory, some signals can contain a substantial amount of noise or do not provide useful information. For example, during the ECGI measurements, some electrodes may have lost contact with the body surface. The electrodes with inadequate signal quality were identified by an automatic check and thereafter by a manual check of the signals. Automatic removal was performed based on the power of the signal. If the power of a signal deviated more than one standard deviation of the median power, the electrode was identified as inadequate. Manual removal of poor signals was performed on the basis of visual inspection. After removal of electrodes with inadequate signal quality, the MUMC+ set-ups consisted of a median of 171 electrodes, with a minimum of 161 electrodes and a maximum of 192 electrodes (Table 1).

Next, the beats of interest were selected manually. For the selected beats, manual selection of the QRS segment and T-wave segment were performed. The T-wave segments were filtered with a second order 40 Hz low-pass Butterworth filter. In total, 60 beats (50 SR beats and 10 VES) were selected (Table 1).

Table 1: Number of electrodes with adequate signal quality in MUMC+ set-ups

Beat	SR1	SR2	SR3	SR4	SR5	VES1	VES2
Patient (total amount of electrodes)							
Patient 1 (182)	163	163	164	165	167	167	167
Patient 2 (184)	172	172	173	168	172	-	-
Patient 3 (184)	170	171	171	174	174	-	-
Patient 4 (184)	170	173	168	176	176	176	-
Patient 5 (184)	168	164	163	164	163	164	163
Patient 6 (184)	163	163	161	161	162	162	-
Patient 7 (215)	188	188	190	190	188	192	-
Patient 8 (184)	177	177	177	178	173	177	179
Patient 9 (184)	162	162	163	163	162	-	-
Patient 10 (184)	174	174	175	174	174	174	-

3.1.3.2. Electrode selection

Selection of electrodes for the different set-ups (Figure 4) was performed manually. The electrode locations in the MUMC+ set-ups did not always match the correct locations for the different set-ups. In some cases, no electrode was present near the correct location. Therefore, selection of electrodes was made on the basis of which selection would visually correspond best to the correct selection. These selections, however, included electrodes with inadequate signal quality (Figure 7). Exclusion of these inadequate electrodes leaves set-ups consisting of different number of electrodes, which does not benefit the comparison. Therefore, all inadequate electrodes were replaced by available electrodes with adequate signal quality, to maintain the number of electrodes. To find a good replacement, the vertical electrode strip of the electrode with inadequate signal quality was automatically checked for electrodes with adequate signal quality within four electrodes above and below the inadequate electrode (Figure 7). If no good replacement within the electrode strip was found, the replacement electrode was manually chosen in electrode strips near the inadequate electrode.

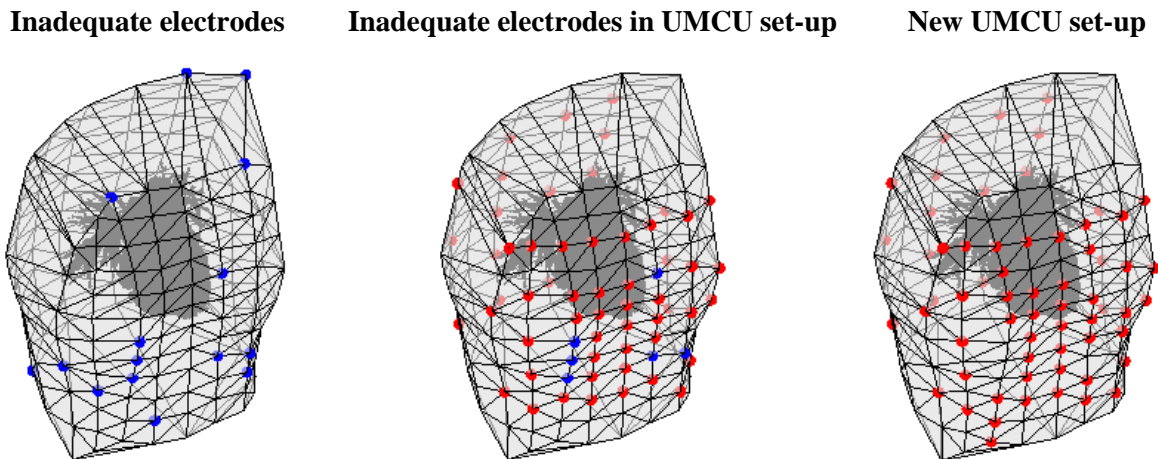


Figure 7: Electrodes with inadequate signal quality are indicated with a blue colour. Electrodes with adequate signal quality are indicated with a red colour. Left) Inadequate electrodes in MUMC+ set-up. Middle) Inadequate electrodes in selected UMCU set-up. Right) New UMCU set-up. Inadequate electrodes are replaced with electrodes with adequate signal quality within the same electrode strips.

3.1.3.3. Inverse reconstruction

The used transfer matrices were generated based on all electrodes of the MUMC+ set-ups (electrodes with inadequate signal quality included), to exclude the effect of the transfer matrix for this simulated inter-system comparison. Inverse reconstructions of the epicardial electrograms were performed on the basis of the PPS model with zero-th order Tikhonov regularization. For AT and RT determination two different methods are possible: the temporal-only approach and spatiotemporal approach. The temporal-only approach determines the AT and RT based on the steepest slope of the local electrogram, whilst the spatiotemporal approach takes into account the electrograms of neighbouring nodes. Currently, the spatiotemporal approach is used for ECGI in the VIGILANCE study, because AT and RT determination are more consistent with simultaneously invasively measured electrograms with the spatiotemporal approach in comparison to the temporal-only approach.⁴² Figure 8 shows the outcome of an inverse reconstruction. Local EGMs were reconstructed for virtual nodes on the epicardium, from which AT and RT were determined.

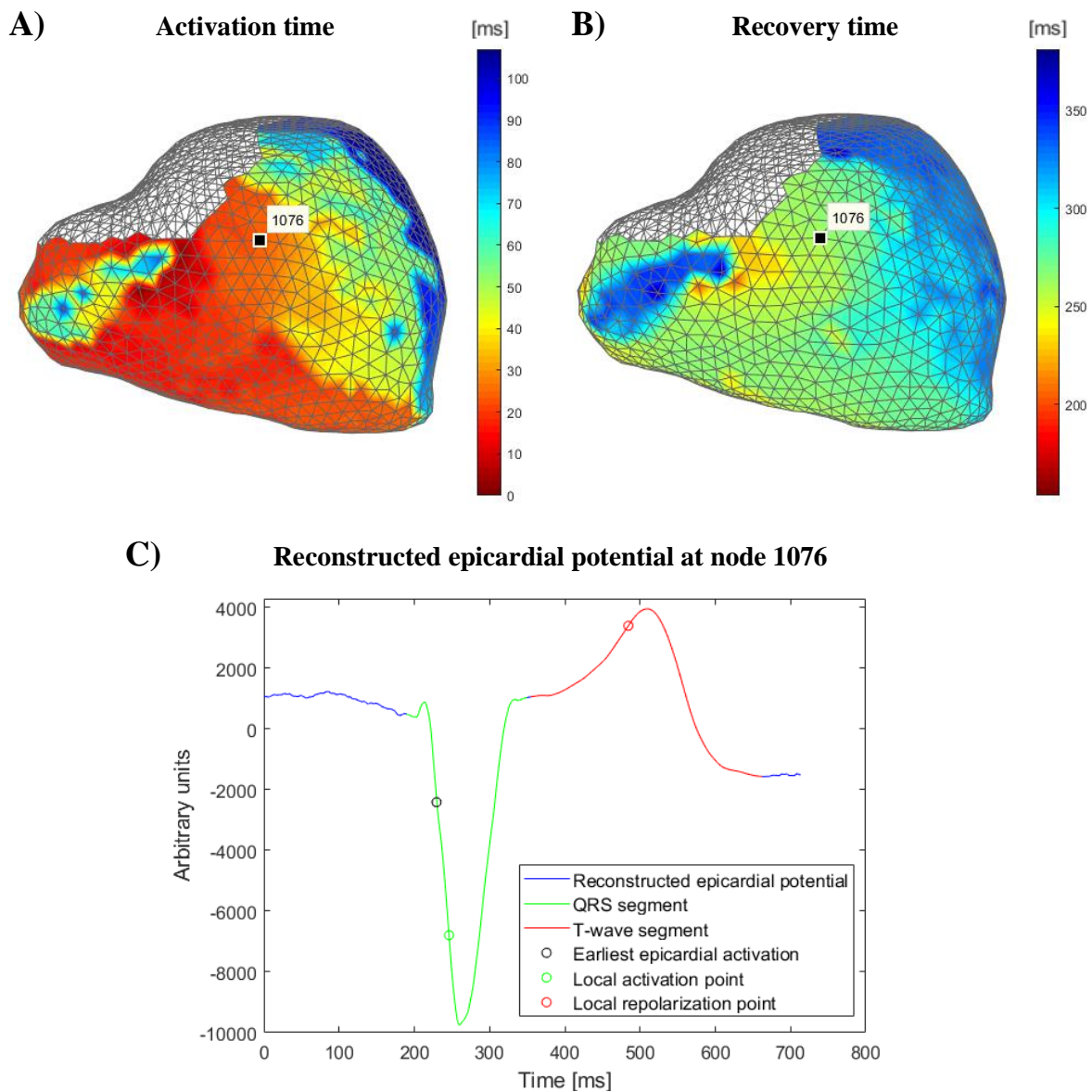


Figure 8: Outcome inverse reconstruction. A) Activation times [ms] are plotted over the epicardium. B) Recovery times [ms] are plotted over the epicardium. C) Reconstructed local electrogram of the node indicated in A and B.

3.1.3.4. Outcome measures

For calculation of the outcome measures, the nodes at the ventricular base (valve plane) were excluded (Figure 8A and B, grey area on epicardium). Selection of the basal nodes was performed in ParaView (Version 5.8.0, Kitware, New York, USA) and checked by visualization of the epicardium with the selected basal nodes and the blood pool in Matlab.

T-wave amplitude & polarity

As can be seen in Figure 8C, the T-waves in the reconstructed EGMs usually contain baseline difference. For correct calculation of the amplitude and determination of the polarity, the baseline difference present in the T-wave segment was removed by subtracting a linear fit. Thereafter, the prominence of the peaks and nadirs in the T-wave segment were determined. The peak or nadir with the largest prominence was considered the T-wave. Therefore, the amplitude was set equal to the largest prominence. If no peak or nadir was found the amplitude was set zero. The polarity was determined positive if the largest prominence was found in a peak, and negative if the largest prominence was found in a nadir. The polarity was defined nor positive nor negative if no peak or nadir was found or when the maximum prominence of the peak and the maximum prominence of the nadir differed only a factor 0.8 or more (biphasic T-wave).

The value of the amplitude is in arbitrary units. Between the reconstructed local EGMs over the heart, large differences in amplitude can exist, which is a known effect in ECGI. A T-wave with low amplitude can have a steep slope and is therefore not necessarily a flat T-wave. Normalization is therefore necessary, in order to interpret the amplitude. The T-wave amplitudes were normalized based on the corresponding QRS amplitudes of the local EGMs.

T-wave correlation

Pearson's correlation coefficients were calculated for the reconstructed epicardial T-wave of the ground truth and the corresponding reconstructed T-wave of the selected set-ups. For flat T-waves noise prevails, causing a lower correlation. However, it does not mean the reconstructed T-waves do not match. Therefore, flat T-waves were excluded for correlation analysis. A T-wave was defined flat if its normalized amplitude was lower than a third of the median of all normalized epicardial amplitudes.

T-wave noise

A signal-to-noise ratio (SNR) was calculated for the local EGM in the T-wave segment per node. The T-wave usually contains frequencies up to 10 Hz.⁵⁶ Therefore, the SNR was calculated as the power of the signal up to 10 Hz divided by the power of the signal.

Activation & recovery duration

The total epicardial activation duration was calculated from the mean of the five earliest ATs to the mean of the five latest ATs of the epicardial nodes. The epicardial recovery duration was determined from the mean of the five earliest RTs to the mean of the five latest RTs of the epicardial nodes.

AT & RT difference

AT and RT depend on the earliest epicardial activation. The earliest epicardial activation is defined as the earliest AT on the epicardium, which is the AT of one node of the ~2000 nodes. Difference in earliest AT between the reconstructions of different electrode set-ups (e.g. the earliest AT of one of the reconstructions is an outlier), leads to a standard difference in the ATs and RTs between the reconstructions, because the earliest AT is removed from all ATs and RTs. However, it does not mean that all AT and RT points are set with a deviation over the epicardium. For the comparison of the reconstructions of different set-ups, it is relevant to know if the AT and RT points are placed in a comparable way. Therefore, the earliest AT was not removed from the AT and RT points. The ATs and RTs are then calculated from the beginning of the beat segment. The beginning of the beat segment differs between the selected beats. However, the differences in AT and RT were all examined within the same beat.

Repolarization gradients

Calculation of the repolarization gradients was already embedded in the inverse reconstruction scripts. The repolarization gradients were calculated per node. First, a median filter was used over a region of 15 mm for each node. Then, the neighbouring nodes within 10 mm of each node were determined. The gradient in RT for a node of interest (NOI) was calculated between the NOI and its neighbours by taking the absolute of the RT of the NOI minus the RT of the neighbour, divided by the distance between the two nodes. The gradient for the NOI was defined as the max gradient in the 10 mm region. The unit of the calculated gradients is ms/cm. Although the gradients were calculated per node, the gradients for different electrode set-ups were not compared node-to-node because of the spatial displacement which can take place. Visually checking the gradients of different reconstructions on the epicardium is time consuming and not accurate. The optimal method to automatically evaluate gradient differences is unknown. Within the VIGILANCE study, the way to quantify gradient differences is not yet defined. Currently, it is being investigated whether to evaluate the gradients of different reconstructions based on differences in the 95th percentile of the gradients on the epicardium. Therefore, in this study the differences in 95th percentile of the gradients were calculated.

3.1.3.5. Post-processing of RTs

Preliminary results of this study showed RT points set in places that were not expected regarding the temporally RT place (steepest positive slope) in the T-wave segment. Based on the used spatiotemporal method, some shift in local RTs was expected. However, when assessing RT points of neighbouring nodes, the incorrect RTs could not always be explained. It is important for correct comparison of the set-ups to minimize and evaluate other factors which can contribute in the arise of differences. For example, noise plays a role in the arise of RT differences. RT point determination is more susceptible to noise than the AT point determination, because of the lower amplitude of the T-wave in comparison to the QRS. Furthermore, differences can arise because correct RT point determination is more difficult in flat or biphasic T-waves.

For better examination on the influence of the number and distribution of electrodes, post-processing of the RTs was implemented. Post-processing consisted of detection and removal of incorrectly placed RT points. Furthermore, the removed RT points were reconstructed by interpolation of correct RTs surrounding the removed RT. Beside benefits for this study, detection of incorrect RTs can improve ECGI in general. Detection of incorrect RTs included two steps. In the first step, RTs present in the first and last ten milliseconds of the T-wave segment were eliminated, because RT points are not expected close to the beginning or end of the selected T-wave segments. The second post-processing step included a newly developed detection method, called the ‘uncertainty score’. This score indicates which RTs still meet the temporal expectations.

Uncertainty score

The uncertainty score was designed to allow automatic detection of uncertain RTs and is based on the derivative of the T-wave. The output of the uncertainty score is binary: an uncertain RT point gets a value of one, whereas a certain RT point gets a value of zero. With the uncertainty score, the RT is defined certain if the x-value is within the largest positive area under the curve (AUC) of the T-wave derivative and uncertain if it is not.

Figure 9 and 10 show the concept of the uncertainty score. In Figure 9, a negative T-wave (blue colour) and its derivative (red colour) are shown. The x-value of the corresponding RT-point (red star) is shown on the $y = 0$ line (black line). Based on the temporal expectation, the RT point should be set in the upslope of the T-wave. Focussing on the derivative, the x-value of RT point should therefore be within the largest positive AUC of the derivative (marked with the black dotted box). In this case, the RT point meets the expectations and therefore receives an uncertainty score of zero.

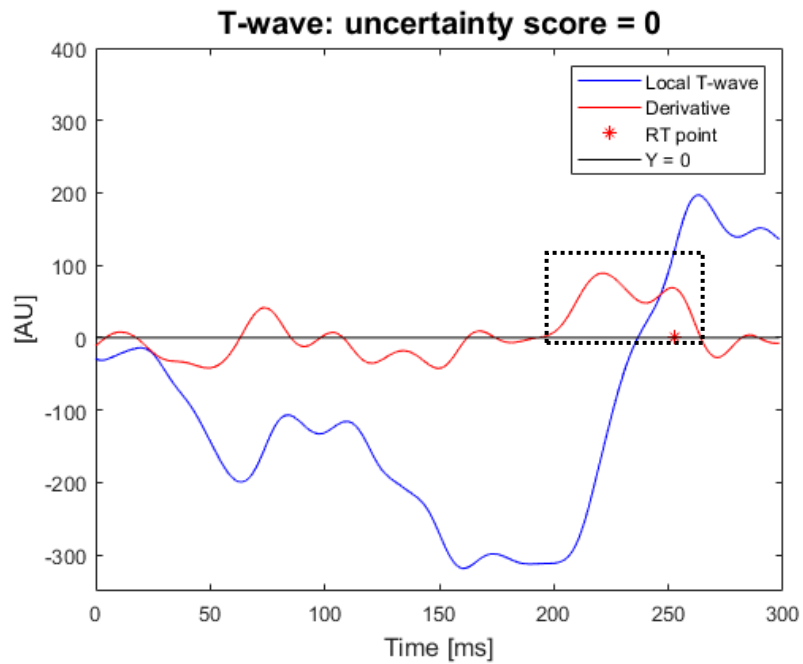


Figure 9: Certain RT point. The largest positive area of the derivative is indicated by the black dotted rectangle. Uncertainty score = 0.

Figure 10 shows a positive T-wave (blue colour) and its derivative (red colour). As can be seen, the RT point does not meet the temporal expectations, as the x-value of the RT point is not set in the upslope of the T-wave. In the case as shown in Figure 10, the RT does not occur inside the largest positive AUC of the derivative and therefore receives an uncertainty score of one.

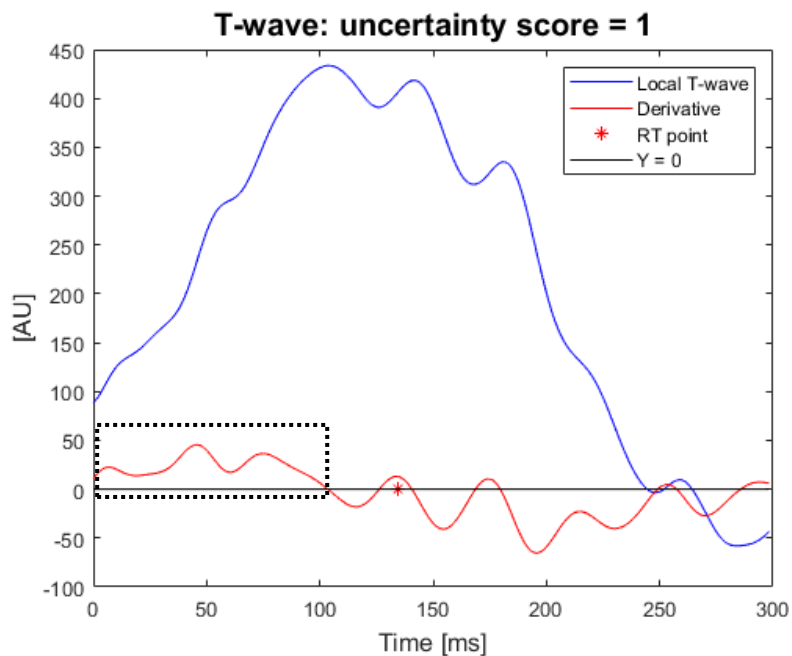


Figure 10: Uncertain RT point. The largest positive area of the derivative is indicated by the black dotted rectangle. Uncertainty score = 1.

Before implementation, the uncertainty score was checked visually by looking at RTs displayed over the epicardium and the local EGMs of a number of reconstructions (Figure 11 and 12). In Figure 11, the uncertainty score and RTs before and after post-processing of a SR beat reconstruction of a patient are visualized over the epicardium. As can be seen, small areas with RTs that deviate from their surroundings are marked by the uncertainty score and are no longer present after post-processing. Furthermore, it was seen that the uncertainty score indicates areas with a polarity transition (biphasic or flat T-waves). It is known that RT determination in those areas is difficult.

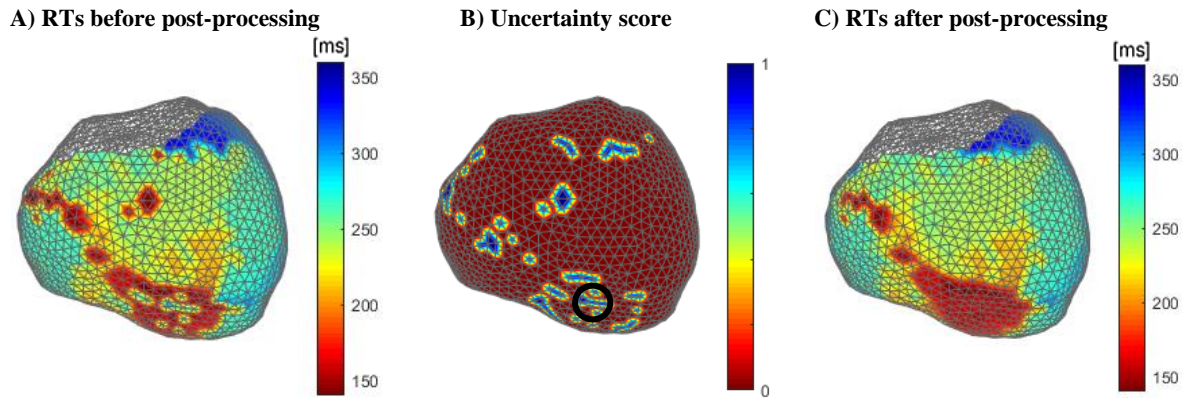


Figure 11: A) RTs in milliseconds before post-processing. B) Uncertainty score: uncertain RT = 1, certain RT = 0. C) RTs in milliseconds after post-processing.

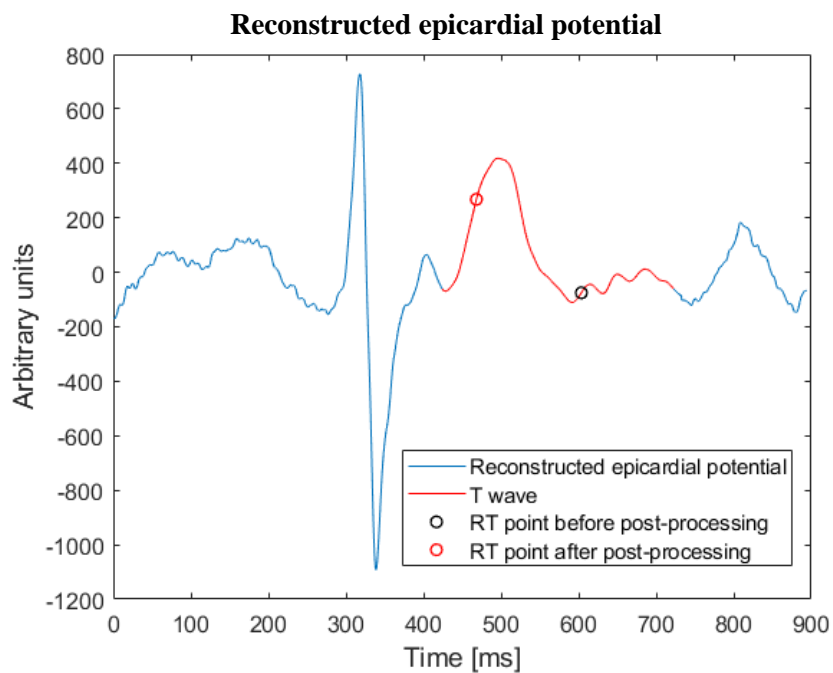


Figure 12: Reconstructed epicardial potential of a node with uncertainty score of 1 in the marked area (black circle) of Figure 9B. In the local T wave (red line), the RT point before post-processing (black circle) and RT point after post-processing (red circle) are displayed.

3.2. Optimal set-up

3.2.1. Study design

The purpose of this sub study was to find the necessary number and positioning of body-surface electrodes for high quality ECGI regarding the assessment of epicardial repolarization differences. For this study the same data as described in methods section 3.1 were used. To investigate the ECGI quality of adjusted set-ups, again a simulated inter-system comparison was performed with the MUMC+ set-up as ground truth. The UMCU set-up was used as fixed set-up, from which electrodes were removed and added. The UMCU set-up is standardized, allowing a standardized approach in removal of electrodes. Furthermore, it is hypothesized that the limit of electrodes necessary for sufficient ECGI quality is below 59 electrodes. To investigate the effect of addition and removal of electrodes, it is therefore interesting to start with this 64-electrodes set-up.

Per adjusted set-up, ten SR beat reconstructions and ten VES reconstructions were made. A lower number of the 50 selected SR beats were used for this sub study because of the duration of a reconstruction (~15 minutes). The reconstructions of the adjusted UMCU set-ups were compared to the reconstructions of the MUMC+ set-up. Comparison of reconstructions was performed based on the T-wave correlation, AT and RT. The study design of this sub study is shown in Figure 13.

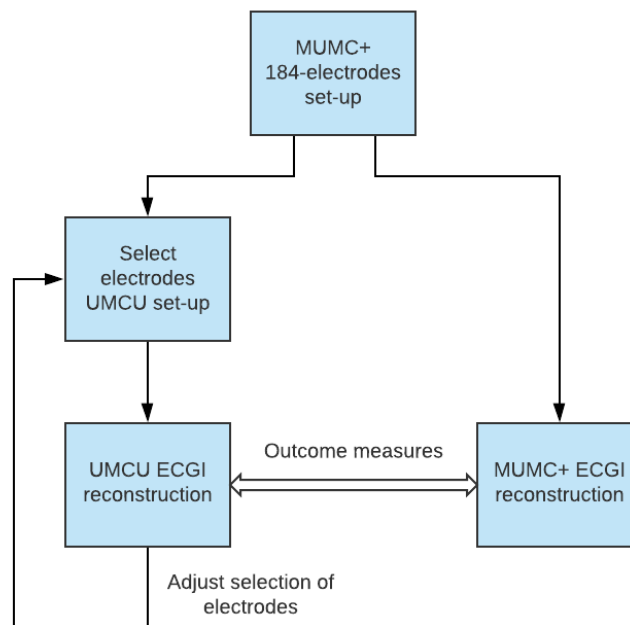


Figure 13: Flowchart of the study design.

3.2.2. Data analysis

The same method for inverse reconstruction and post-processing of RTs was used as described in methods section 3.1. However, for this study the reconstructions were made for a selected number of beats and other electrode set-ups.

3.2.2.1. Beat selection

For the VES reconstructions of this study, the same ten VES were used as in Table 1. For the SR beat reconstructions, ten SR beats were selected from the 50 SR beats in Table 1. For each patient one SR beat was selected. Selection of the SR beat was based on the largest number of electrodes with adequate signal quality per patient (Table 1). In this way, the widest choice of electrodes was retained for the addition of electrodes. The used SR beats and their number of adequate electrodes in the MUMC+ set-up are shown in Table 2.

Table 2: Used SR beats with their number of electrodes with adequate signal quality in the MUMC+ set-ups.

	Used SR beat (Table 1)	Number of electrodes with adequate signal quality in MUMC+ set-up of used SR beat
Patient 1	SR5	167
Patient 2	SR3	173
Patient 3	SR4	174
Patient 4	SR4	176
Patient 5	SR1	168
Patient 6	SR1	163
Patient 7	SR3	190
Patient 8	SR4	178
Patient 9	SR3	163
Patient 10	SR3	175

3.2.2.2. Removal of electrodes

Creation of adjusted UMCU set-ups with a lower number of electrodes was performed by iterative removal of one vertical or horizontal row of electrodes. The vertical rows and horizontal rows which were removed are shown in Figure 14. In total, seventeen different set-ups were created. The vertical rows consist of three to seven electrodes and the horizontal rows of twelve electrodes. Therefore, the minimal set-ups consisted of 52 electrodes.

When removing strips of electrodes, care was taken to the replaced inadequate electrodes of the original UMCU set-ups. For removal of a UMCU set-up strip which contained an inadequate electrode, no replacement electrode had to be included in the set-up. However, if the electrode strip was removed which contained the replacement for another strip, a new replacement was sought.

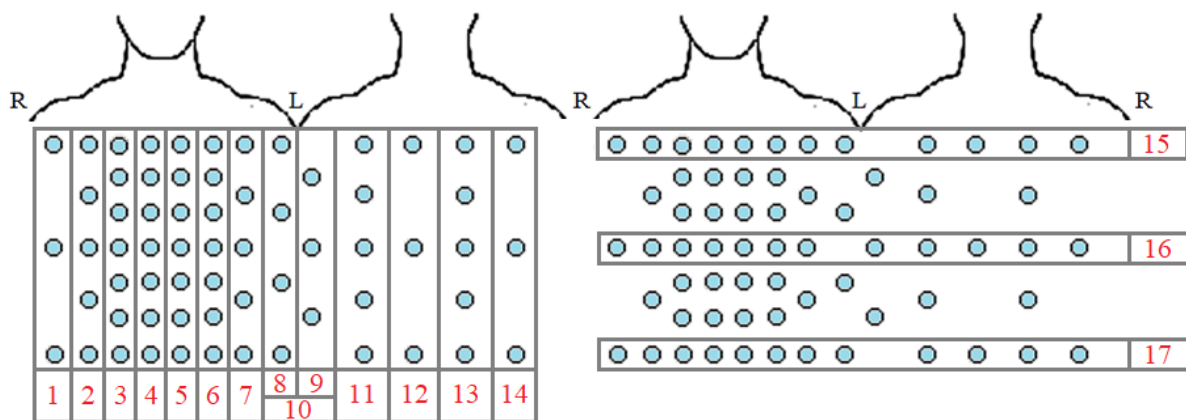


Figure 14: Schematic representation of the remove steps. Step 1 t/m 14: removal of a vertical row of electrodes of the UMCU set-up. Step 15 t/m 17: removal of a horizontal row of 12 electrodes of the UMCU set-up.

3.2.2.3. Addition of electrodes

Creation of adjusted UMCU set-ups with a higher number of electrodes was performed by adding electrodes. The electrodes for addition were manually selected. First, it was checked which addition options were possible to perform for each original UMCU set-ups, since the MUMC+ set-up is not standardized and inadequate electrodes were excluded. In total, seven adjusted UMCU set-ups were created (Figure 15)

For the first and second adjusted set-up a row of ten electrodes was added superior and inferior to the original UMCU set-up, respectively. For the third adjusted set-up both the superior and inferior row were added, which created set-ups of 84 electrodes. For adjusted set-up four to seven, five electrodes were added to the four different anterior quadrants of the thorax, creating four adjusted set-ups of 69 electrodes. The electrode selection was made based on the available electrodes and a roughly even distribution. The MUMC+ set-up of patient 6 lacked electrodes with adequate signal quality inferior of the thorax to be able to perform addition step 2, 3, 6 and 7. Therefore, the adjusted set-ups for which electrodes were added inferior were not created for patient 6.

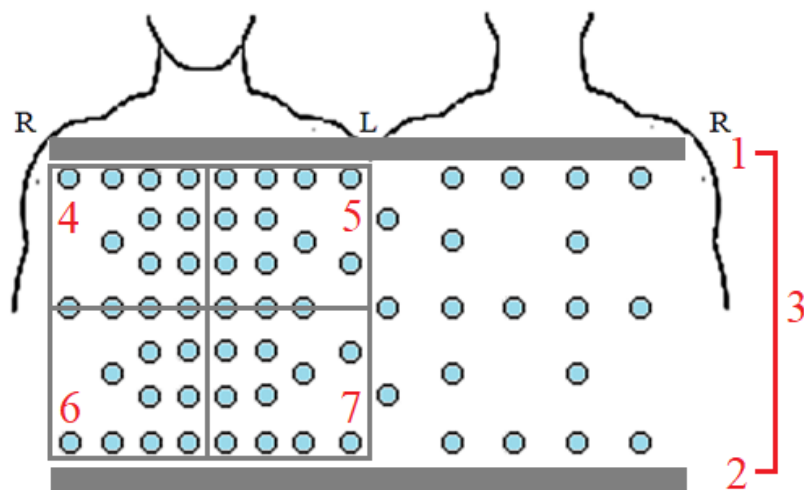


Figure 15: Schematic representation of the addition steps. Step 1: Row of ten electrodes superior of the UMCU set-up. Step 2: Row of ten electrodes inferior of UMCU set-up. Step 3: Step 1 and 2. Step 4, 5, 6 and 7: addition of five electrodes to each quadrant of the anterior thorax.

At last a set-up of 100 electrodes was created, to compare the results to a larger set-up. This set-up consisted of 55 electrodes anterior, five electrodes at each lateral side and 35 electrodes at the posterior side of the thorax.

3.2.2.4. Optimal set-up

Based on the results, the needed location and number of electrodes for an optimal set-up were investigated. In order to investigate the lower limit, horizontal or vertical rows of electrodes, which did not affect the ECGI quality when left out, were removed in addition to one another, while taking into account the important locations. In addition, it was investigated if a more optimal distribution could be found for the 64 electrodes of the original UMCU set-up. Change in distribution was performed by replacement of the electrode rows with small effect on the ECGI quality after removal, to locations which seem to improve the ECGI quality.

4. Results

4.1. Current set-ups

4.1.1. T-wave correlation

The median T-wave correlation coefficient for the MUMC+ set-up with the UMCU, Amsterdam UMC and standard 9-electrodes set-up are shown in Table 3. In general, high correlation coefficients were found for the UMCU-MUMC+ and Amsterdam UMC-MUMC+ comparison, for both SR beats and VES. The median T-wave correlation coefficient for the standard 9-electrodes-MUMC+ comparison was lower. Focussing on the first quartile and third quartile of the MUMC+ - standard 9-electrodes comparison, epicardial regions with high correlation coefficients were present, but also regions with poor correlation were found.

It is apparent from Table 3 that the UMCU set-up results in the highest overall T-wave correlation coefficients. Furthermore, the median correlation coefficient of patient 6 for the Amsterdam UMC-MUMC+ comparison stands out. The reconstructed EGMs of the Amsterdam UMC reconstructions of this patient correspond poorly to the reconstructed EGMs of the MUMC+ reconstructions.

Table 3: Median correlation coefficient of the T-wave for different set-ups and beats.

Median correlation coefficient T-wave (Q1 – Q3)	UMCU-MUMC+	Amsterdam UMC- MUMC+	Standard 9-MUMC+
5 SR beats patient 1	0.94 (0.80 – 0.98)	0.99 (0.94 – 1.00)	0.84 (-0.20 – 0.97)
5 SR beats patient 2	0.98 (0.92 – 0.99)	0.96 (0.88 – 0.99)	0.87 (0.00 – 0.96)
5 SR beats patient 3	0.97 (0.92 – 0.99)	0.95 (0.87 – 0.98)	0.89 (0.51 – 0.97)
5 SR beats patient 4	0.97 (0.87 – 0.99)	0.91 (0.71 – 0.98)	0.68 (0.27 – 0.92)
5 SR beats patient 5	0.99 (0.97 – 1.00)	0.99 (0.96 – 1.00)	0.91 (0.49 – 0.97)
5 SR beats patient 6	0.96 (0.67 – 0.99)	0.04 (-0.42 – 0.52)	0.72 (-0.25 – 0.94)
5 SR beats patient 7	0.98 (0.88 – 0.99)	0.91 (0.57 – 0.98)	0.77 (0.01 – 0.95)
5 SR beats patient 8	0.97 (0.92 – 0.99)	0.94 (0.82 – 0.98)	0.53 (-0.81 – 0.92)
5 SR beats patient 9	0.99 (0.97 – 1.00)	0.99 (0.96 – 1.00)	0.90 (0.71 – 0.97)
5 SR beats patient 10	0.98 (0.94 – 0.99)	0.97 (0.92 – 0.99)	0.89 (0.41 – 0.97)
SR (50 in total)	0.98 (0.92 – 0.99)	0.96 (0.88 – 0.99)	0.85 (0.14 – 0.97)
VES (10 in total)	0.98 (0.91 – 1.00)	0.97 (0.87 – 0.99)	0.83 (0.11 – 0.96)

4.1.2. Activation and recovery time

Figure 16 shows violin plots with node-to-node absolute AT and RT differences for the reconstructions of the UMCU, Amsterdam UMC and standard 9-electrodes set-ups compared to the reconstructions of the MUMC+ set-up. Per graph, ten violin plots show the node-to-node differences collected of the 5 SR beats per patient and one violin plot shows the differences collected of the ten VES. The width of the violin plots indicate the occurrence rate of a certain difference. Overall, larger RT differences were found compared to AT, as expected given the large difference in voltage between the QRS complex and the T-wave and the longer duration of the repolarization compared to the depolarization.

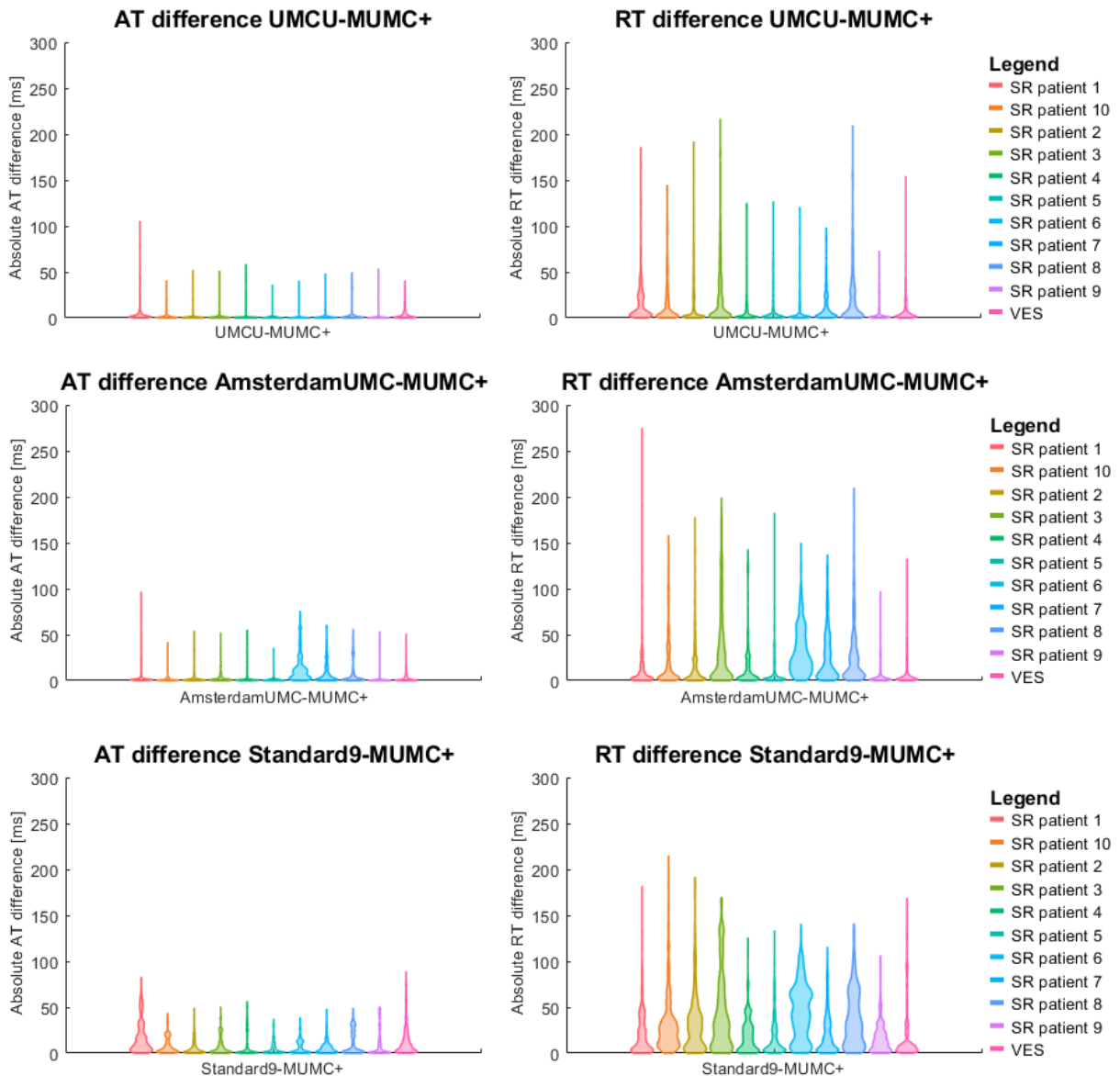


Figure 16: Violin plots of the node-to-node absolute AT and RT differences between the reconstructions of the MUMC+ set-up and the UMCU, Amsterdam UMC and standard 9-electrodes set-up reconstructions.

Focussing on the UMCU-MUMC+ comparison, the absolute AT differences were small. However, outliers were present (Figure 16). The median absolute AT difference was 0.5 ms for SR beats and 1.9 ms for VES. In comparison to the AT, larger RT differences were found (Figure 16). The median absolute RT difference for SR beats was 4.1 ms and for VES 3.4 ms.

For the Amsterdam UMC-MUMC+ comparison, the absolute AT and RT differences of the SR beat reconstructions were in general larger than for the UMCU-MUMC+ comparison (Figure 16). As can be seen in Figure 16, patient 6 shows large AT differences, which are not seen for the other patients. Focussing on the RT, patient 3, 6, 7 and 8 show a wide range of RT differences (Figure 16). The median absolute AT difference for SR beats was 1.0 ms and for VES 1.4 ms. The median absolute RT difference was 7.3 ms for SR beats and 2.9 ms for VES.

Between the reconstructions of the standard 9-electrodes set-up and the MUMC set-up the largest absolute AT and RT differences were found (Figure 16). The median absolute AT difference for SR beats was 3.7 ms and for VES 8.0 ms. The median absolute RT difference was 20.3 ms for SR beats and 7.3 ms for VES. As can be seen in Figure 16, the violin plots are wide over a large range of RT differences, indicating substantial differences in the node-to-node RTs of the MUMC and standard 9-electrode reconstructions.

4.1.3. Activation and recovery duration

Table 4 shows the mean absolute difference in activation duration for the different set-up comparisons. The activation durations found for the reconstructions were around 60 ms for SR beats and 95 ms for VES. As can be depicted from Table 4, the UMCU set-up reconstructions showed the smallest overall differences in mean activation duration with the MUMC+ set-up reconstructions. For the Amsterdam UMC set-up the mean differences were slightly larger. Patient 6 of the Amsterdam UMC set-up showed the largest absolute difference, which is in line with the larger node-to-node absolute AT differences of patient 6 as seen in Figure 16. The difference found for SR beats for the standard 9-electrodes set-up did not differ much from that of the Amsterdam UMC set-up. However, for VES a larger difference in mean absolute activation duration was found.

Table 4: Mean absolute difference in activation duration between the MUMC+ reconstructions and the UMCU, Amsterdam UMC and standard 9-electrode set-up reconstructions.

Mean absolute difference in activation duration [ms]	UMCU-MUMC+	Amsterdam UMC-MUMC+	Standard 9-MUMC+
SR beats (5 per patient)			
Patient 1	4.1	2.2	2.0
Patient 2	2.6	2.8	11.2
Patient 3	2.5	2.9	9.6
Patient 4	8.7	11.6	11.6
Patient 5	3.3	3.1	3.5
Patient 6	6.0	34.8	6.0
Patient 7	1.5	8.9	4.5
Patient 8	2.8	5.1	8.9
Patient 9	2.8	3.6	15.6
Patient 10	3.7	2.4	6.8
Mean of SR beats	3.8	7.7	8.0
VES (10 in total)	4.9	7.3	17.8

The mean absolute difference in recovery duration for the different set-up comparisons is shown in Table 5. The recovery durations found for the reconstructions were around 200 ms for SR beats and 210 ms for VES. Focussing on the mean of all SR beats and VES (Table 5), the absolute differences in recovery duration for the UMCU and Amsterdam UMC set-up were roughly similar. A doubling of the mean difference was found for the standard 9-electrode set-up. Noticeably, for a number of patients for

both the UMCU and Amsterdam UMC set-up, differences comparable to the mean absolute difference of the standard 9-electrodes set-up were found (e.g. patient 4).

Table 5: Mean absolute difference in recovery duration between the MUMC+ reconstructions and the UMCU, Amsterdam UMC and standard 9-electrode set-up reconstructions.

Mean absolute difference in recovery duration [ms]	UMCU-MUMC+	Amsterdam UMC-MUMC+	Standard 9-MUMC+
SR beats (5 per patient)			
Patient 1	14.5	22.1	47.6
Patient 2	19.0	22.6	24.0
Patient 3	8.1	10.1	39.2
Patient 4	26.2	27.4	32.3
Patient 5	8.8	4.5	18.8
Patient 6	8.3	11.6	6.5
Patient 7	18.5	15.7	21.4
Patient 8	10.4	3.9	27.4
Patient 9	7.1	9.0	14.7
Patient 10	26.4	20.5	48.9
Mean of SR beats	14.7	14.7	28.1
VES (10 in total)	12.2	16.6	28.4

Interestingly, the differences in absolute activation and recovery duration fluctuate greatly for different patients. For some patients the differences were even lowest for the standard 9-electrodes set-up, while it consists of the fewest number of electrodes.

4.1.4. Repolarization gradients

Table 6: Mean absolute difference in 95^e percentile of the gradients between the MUMC+ reconstructions and the UMCU, Amsterdam UMC and standard 9-electrode set-up reconstructions.

Mean absolute difference in 95 ^e percentile of the gradients [ms/cm]	UMCU-MUMC+	Amsterdam UMC-MUMC+	Standard 9-MUMC+
SR beats (5 per patient)			
Patient 1	20.3	9.2	35.5
Patient 2	23.0	26.7	37.3
Patient 3	34.3	63.4	39.8
Patient 4	38.3	58.1	131.1
Patient 5	6.9	10.3	14.0
Patient 6	19.8	17.7	30.8
Patient 7	3.8	46.2	72.2
Patient 8	11.5	15.9	55.6
Patient 9	9.6	11.5	16.3
Patient 10	35.6	21.4	17.3
Mean of SR beats	20.3	28.0	45.0
VES (10 in total)	28.3	21.4	50.4

Table 6 shows the mean absolute differences in 95^e percentile of the repolarization gradients. The mean absolute difference was lowest for the UMCU set-up when focussing on the mean of all SR beats. When

focussing on the mean of the VES, the Amsterdam UMC set-up showed the lowest mean difference. The mean absolute difference of all SR beats and VES was highest for the standard 9-electrodes set-up. Thus, the results of all patients together showed that the reconstructed gradients correspond less with the gradients of the MUMC+ set-up if the used set-up consisted of fewer electrodes. However, as with the activation and recovery duration, large fluctuations in absolute differences were seen between the patients.

4.1.5. Regional differences

Visualization of the repolarization-focused outcome measures on the epicardium provides insight into the repolarization differences. The T-wave correlation coefficients and RT differences for each node on the epicardium were visualized for the three comparisons as shown in Figure 17. Figure 18 shows the repolarization focussed outcome measures for the four different set-ups visualized on the epicardium. In general, the epicardial visualizations of the outcome measures for the UMCU and Amsterdam UMC reconstructions had good agreement with the MUMC+ reconstructions. Furthermore, the larger differences in outcome measures for the standard 9 - MUMC+ comparison were clearly visible. Noticeably, the gradients of the reconstructions of the standard 9-electrode set-up were often not well matched in terms of location and size compared to the MUMC+ reconstructions.

The visual inspection revealed that differences between the reconstructions are mainly found at regions with T-wave polarity transition. As can be depicted from Figure 17 and 18, the region with lower T-wave correlation and larger RT differences corresponds to the region in which the T-wave polarity switched and lower normalized T-wave amplitudes were found. Furthermore, the visualisations seemed to show presence of small spatial displacement of reconstructions, which could also result in correlation and RT differences in the area of T-wave polarity transition.

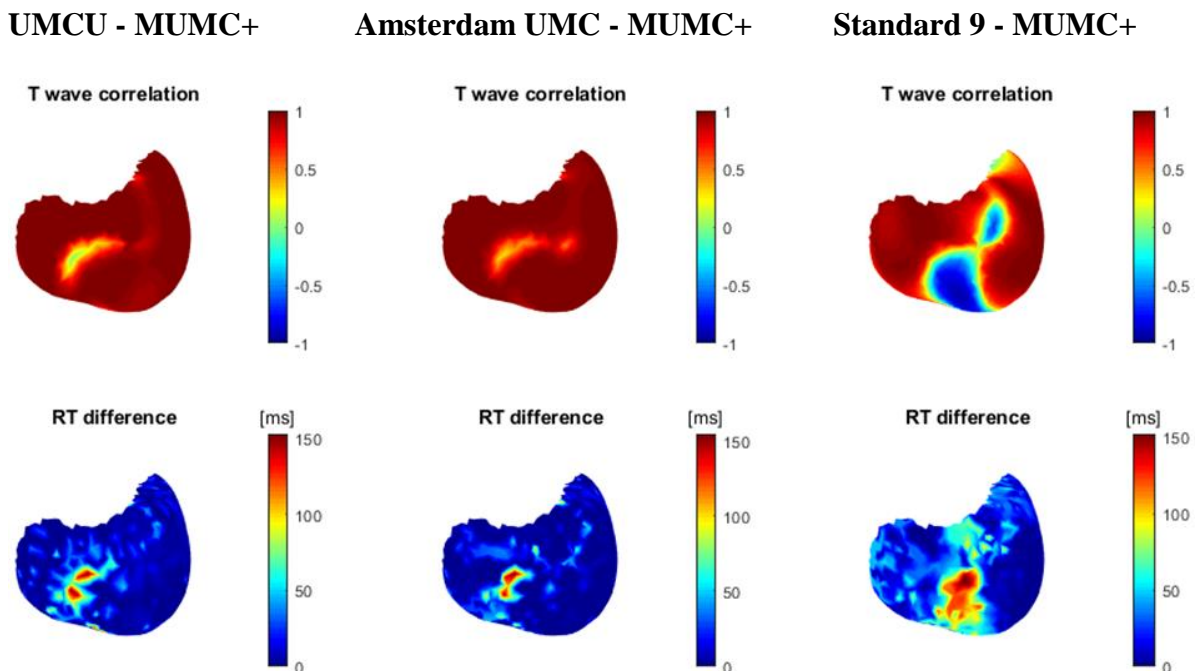


Figure 17: T-wave correlation and absolute RT difference between the MUMC+ reconstruction and the UMCU, Amsterdam UMC and standard 9-electrode set-up reconstruction of a SR beat of patient 9 visualized on the epicardium (anterior view).

MUMC+ set-up

UMCU set-up

Amsterdam UMC set-up

Standard 9-electrodes set-up

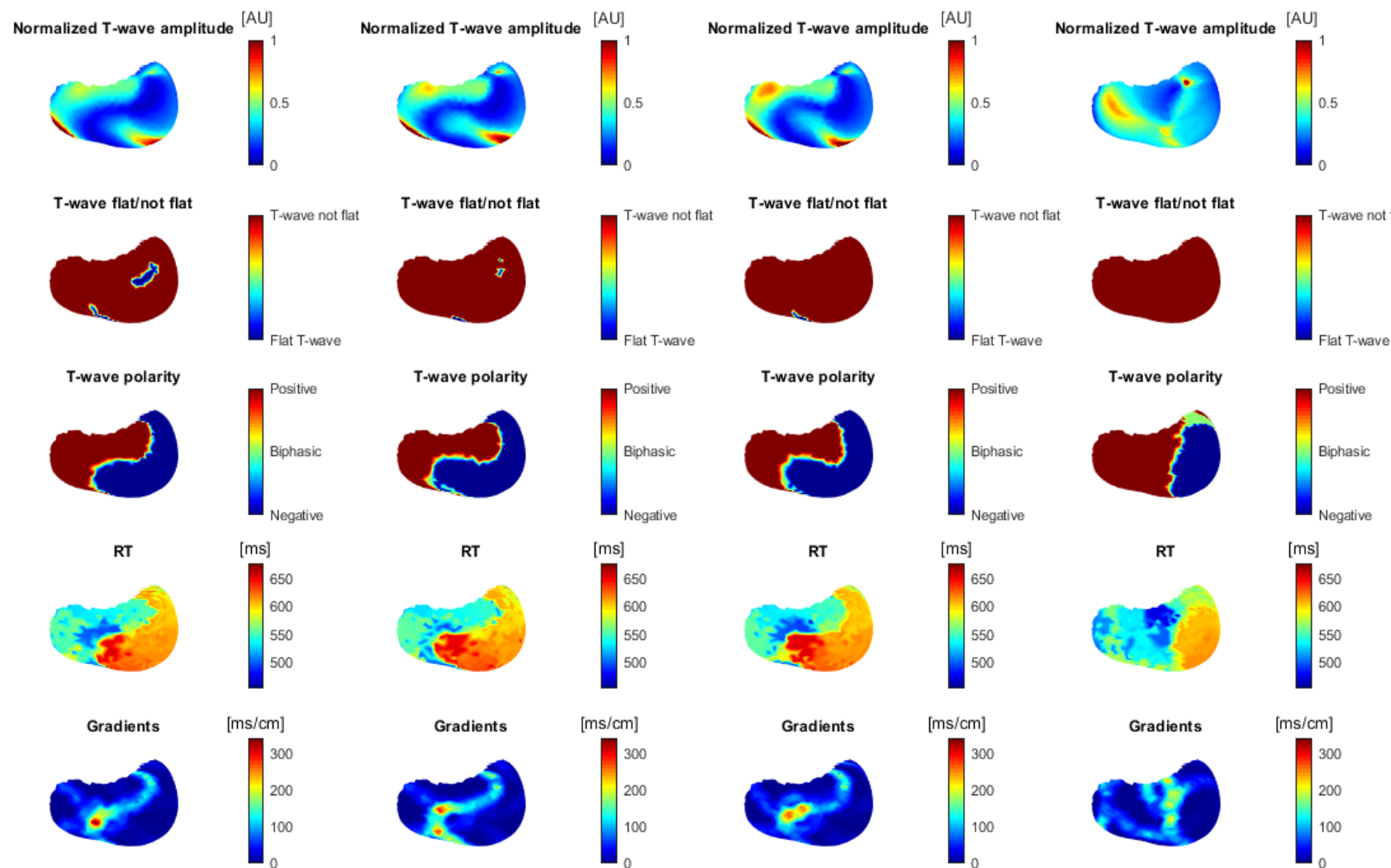


Figure 18: Repolarization focussed outcome measures of a SR beat reconstruction of patient 9 for the MUMC+, UMCU, Amsterdam UMC and standard 9-electrodes set-up visualized on the epicardium (anterior view).

Inspection of the local EGMs in epicardial regions with repolarization differences revealed possible causes for the differences. The local EGM of a node in the area of large RT difference for the UMCU-MUMC+ comparison in Figure 17 (red area) is shown for the MUMC+ reconstruction and UMCU reconstruction in Figure 19. As can be seen from Figure 19, the RT difference and low T-wave correlation were caused by the low amplitude of the reconstructed T-wave.

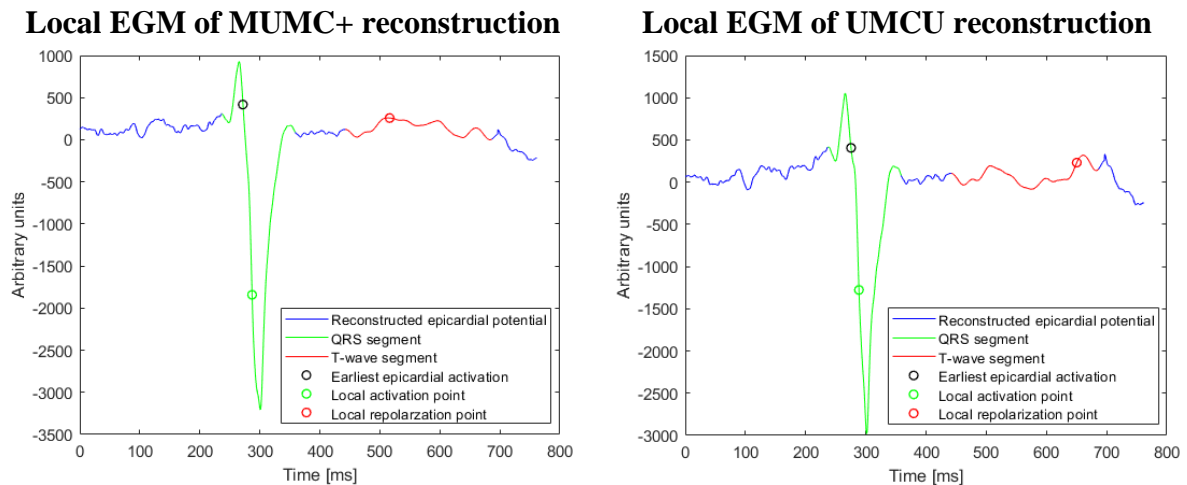


Figure 19: Reconstructed local electrogram of a node in the region with large RT difference (red area in in the lower left panel of Figure 17) of (Left) the MUMC+ reconstruction of patient 9 (Right) the UMCU reconstruction of patient 9.

In addition, areas of differences were found not particularly at the border zone of T-wave polarity transition. Figure 20 and 21 show the repolarization-focused outcome measures visualized on the epicardium for a SR beat of patient 3. In Figure 20, the region with large RT differences for the UMCU-MUMC+ comparison stands out. In Figure 21, it can be seen that in this region the RTs were higher for the MUMC+ reconstruction and lower for the UMCU reconstruction in comparison to the surrounding nodes. In this particular region, the amplitude and polarity of the T-waves also differed for the MUMC+ and UMCU reconstruction. Focussing on the gradients, it can be seen that the gradients for the MUMC+, UMCU and Amsterdam UMC had roughly the same spatial distribution. However, the gradients differed in magnitude.

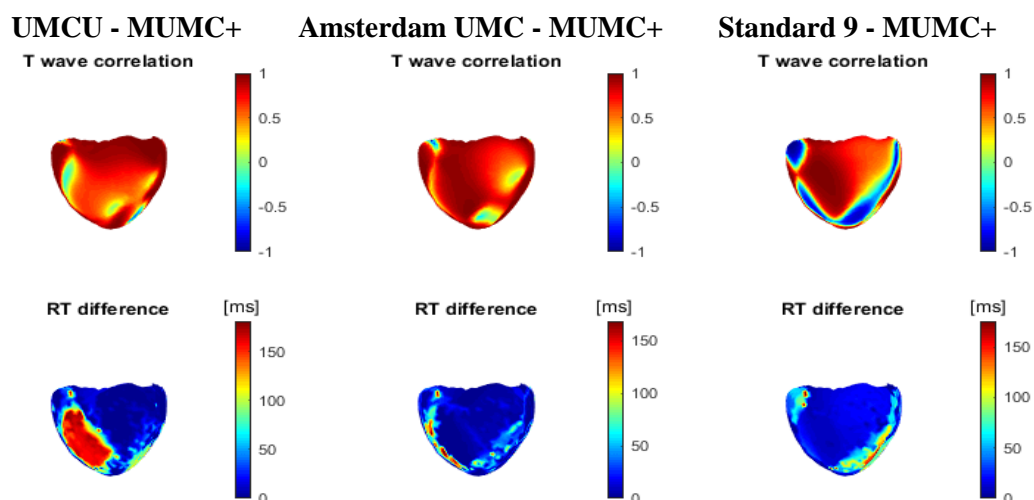


Figure 20: T-wave correlation and absolute RT difference between the MUMC+ reconstruction and the UMCU, Amsterdam UMC and standard 9-electrode reconstruction of patient 3 visualized on the epicardium (posterior view).

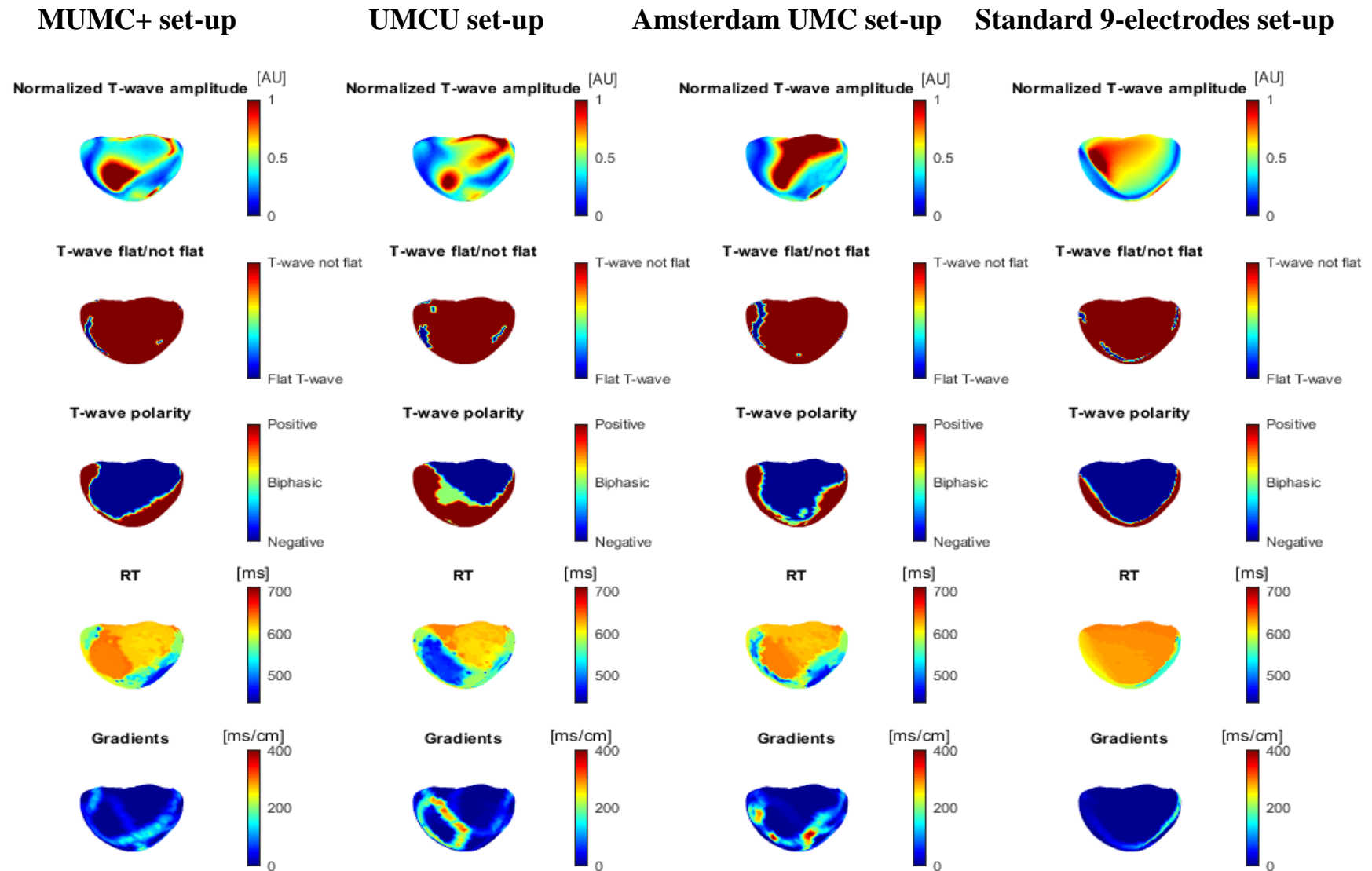


Figure 21: Repolarization focussed outcome measures of a SR beat reconstruction of patient 3 for the MUMC+, UMCU, Amsterdam UMC and standard 9-electrodes set-up visualized on the epicardium (posterior view)

The local EGM of a node in the epicardial region of large RT difference between the MUMC+ and the UMCU reconstruction is shown in Figure 22 for every set-up. The EGM of the MUMC+ and UMCU reconstruction confirmed the difference in RT and T-wave polarity. Although the T-wave for the Amsterdam UMC and standard 9-electrodes reconstructions were more comparable to the T-wave of the MUMC+ reconstruction, the rest of the local EGMs were inconsistent. Interestingly, the EGMs in the areas with different reconstructed EGMs had lower magnitudes. Figure 23 shows the EGM correlation between the MUMC+ and UMCU reconstruction (left figure) and the normalized magnitude of the local EGMs of the MUMC+ reconstruction (right figure) of the same SR beat of patient 3 visualized on the epicardium. The EGM magnitudes were determined as the heights of the absolute EGMs normalized by the highest EGM height on the epicardium. As can be depicted from Figure 23, the reconstructed EGMs were less similar in areas of low magnitude EGMs.

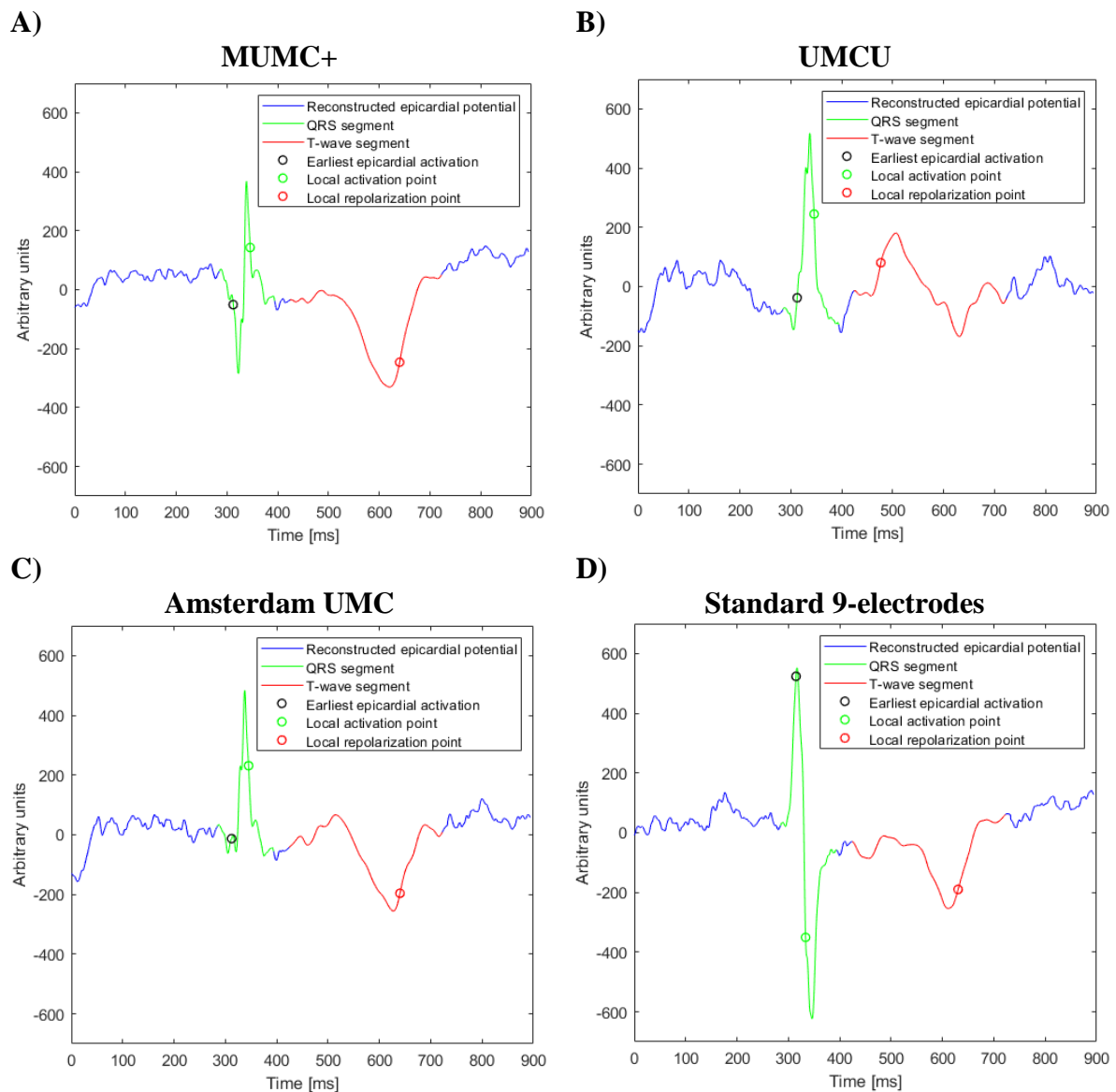


Figure 22: Reconstructed local electrogram of a node in the region with large RT difference (red area in the lower left panel of Figure 20) of patient 3 of (A) the MUMC+ reconstruction (B) the UMCU reconstruction (C) the Amsterdam UMC reconstruction (D) the standard 9-electrodes reconstruction.

EGM correlation UMCU-MUMC+

Normalized magnitude MUMC+ EGMs

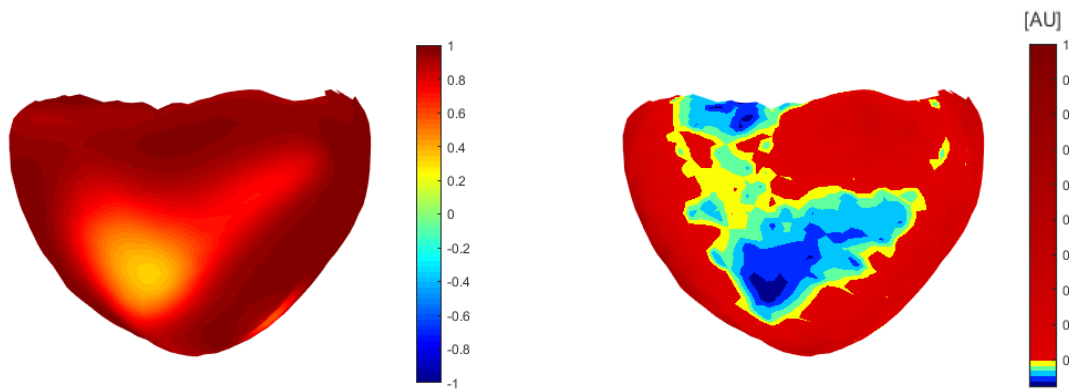


Figure 23: Left) Local electrogram correlation between the MUMC+ and the UMCU reconstruction of patient 3 visualized on the epicardium (posterior view). Right) Normalized EGM magnitude of the MUMC+ reconstruction of patient 3 visualized on the epicardium (posterior view)

The violin plots of Figure 16 showed large absolute RT differences for patient 6 between the MUMC+ and Amsterdam UMC reconstructions. Visual inspection of the outcome measures of the Amsterdam UMC reconstruction on the epicardium showed abnormal T-wave patterns in comparison to the reference MUMC+ reconstruction. Investigation of the cause of these differences showed a difference in the Tikhonov parameter used for regularization. The Tikhonov parameters used for the Amsterdam UMC reconstructions of patient 6 were in the range of 10^{-4} to 10^{-8} , while for the other reconstructions the Tikhonov parameters were in the range of 10^{-3} . Figure 24 shows several outcome measures visualized on the epicardium for a SR beat of patient 6 for the MUMC+ reconstruction, Amsterdam UMC reconstruction with its original Tikhonov parameter choice and an Amsterdam UMC reconstruction with a Tikhonov parameter set at $5.1 \cdot 10^{-3}$.

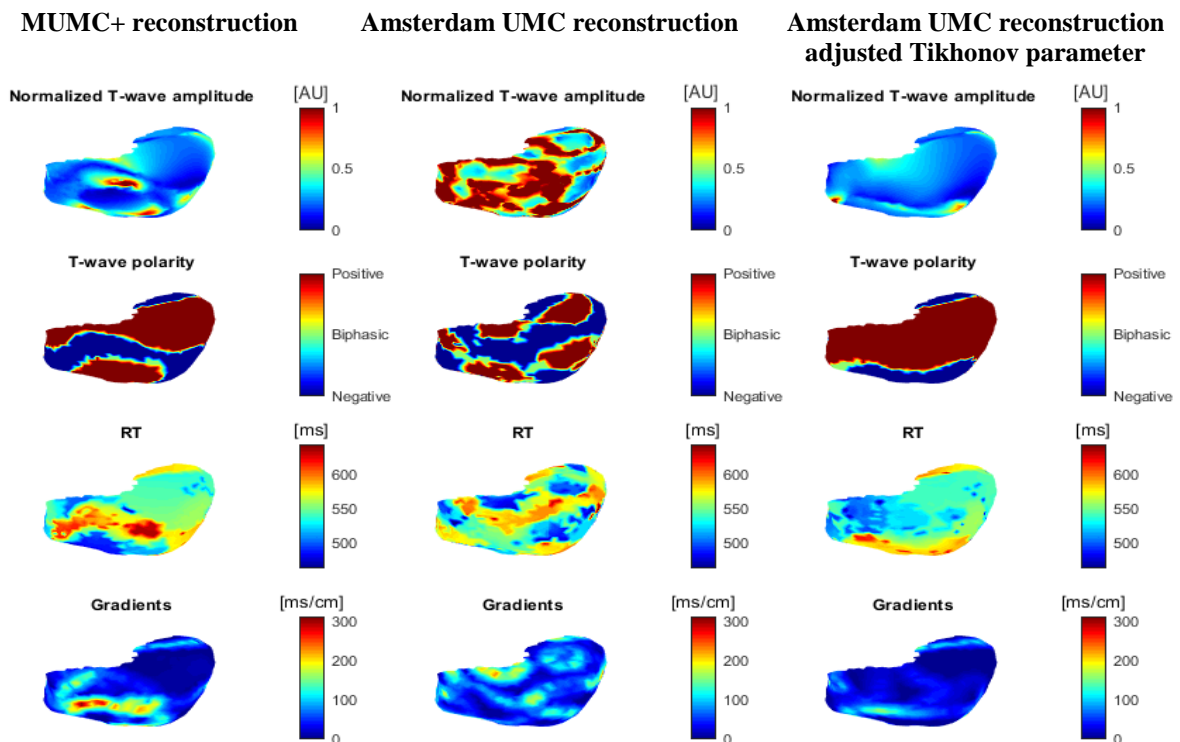


Figure 24: Repolarization focussed outcome measures of patient 6 for the MUMC+ reconstruction and the Amsterdam UMC reconstruction with and without adjusted Tikhonov parameter, visualized on the epicardium (anterior view)

4.1.6. Effect of amplitude and noise

For further investigation of the influence of the T-wave amplitude, EGM magnitude and T-wave noise, the SNR, normalized T-wave amplitude and normalized EGM magnitude of the MUMC+ reconstructions were plotted against the absolute RT differences and T-wave correlation coefficients. Figure 25, 26 and 27 all show the absolute RT differences and T-wave correlation coefficients of the MUMC+-UMCU comparison of a SR beat of patient 7.

Figure 25 shows the influence of the normalized T-wave amplitude on the absolute RT difference and T-wave correlation. It can be seen from Figure 25 that larger RT differences and lower T-wave correlation coefficients were found for lower T-wave amplitudes. Some differences between the reconstructions of the different electrode set-ups can therefore be explained by the T-wave amplitude. It is apparent from the right graph of Figure 25 that for low normalized T-wave amplitudes also high correlation coefficients can be found.

Influence of T-wave amplitude on the RT difference and T-wave correlation

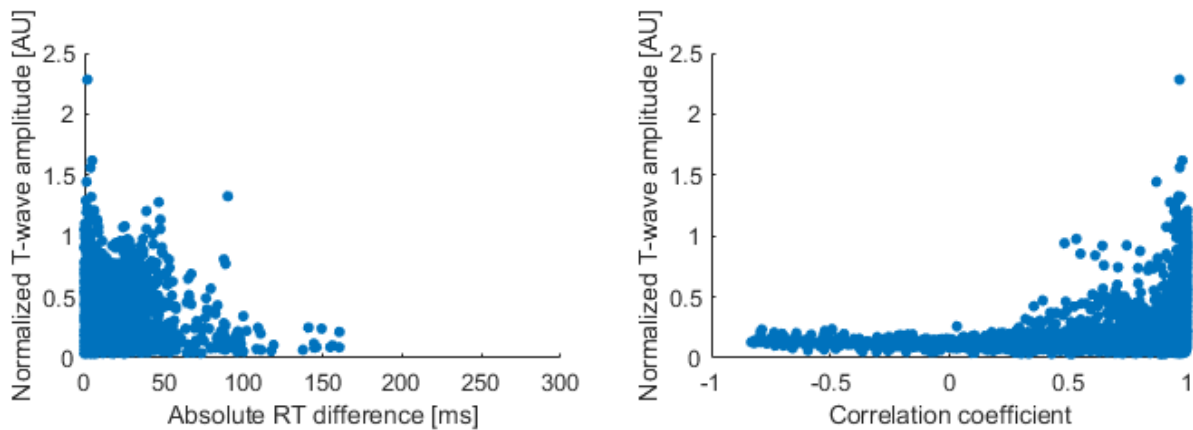


Figure 25: Normalized MUMC+ T-wave amplitudes of the SR beats of patient 8 plotted against (Left) the absolute RT differences for the UMCU-MUMC+ comparison of the SR beats of patient 8 (Right) the T-wave correlation coefficients for the UMCU-MUMC+ comparison of the SR beats of patient 8.

Figure 26 shows the influence of the normalized EGM magnitude on the absolute RT difference and T-wave correlation. It can be seen for patient 8 that large RT differences were more common for EGMs with low magnitude. However, large RT differences also occurred for high magnitude EGMs. For the T-wave correlation a clear trend was visible, indicating lower T-wave correlation coefficients for EGMs with lower magnitudes. Differences in the reconstructed T-waves in areas with low EGM magnitudes can possibly be explained by the ECGI technique. With ECGI, the reconstruction consists of the epicardial EGMs which physiologically best explain the measured body surface potentials. Low voltage epicardial regions may be less decisive for the best fitting reconstruction. Therefore, the reconstructed EGMs in these regions may be more likely to differ for different reconstructions.

Figure 27 shows the influence of noise in the T-wave segment on the absolute RT difference and T-wave correlation. In the left graph of Figure 27 it can be seen that large RT differences were not particularly found if more noise was present in the T-wave segment (lower SNR). Furthermore, no clear trend was found between the SNR and T-wave correlation coefficients.

Influence of EGM magnitude on the RT difference and T-wave correlation

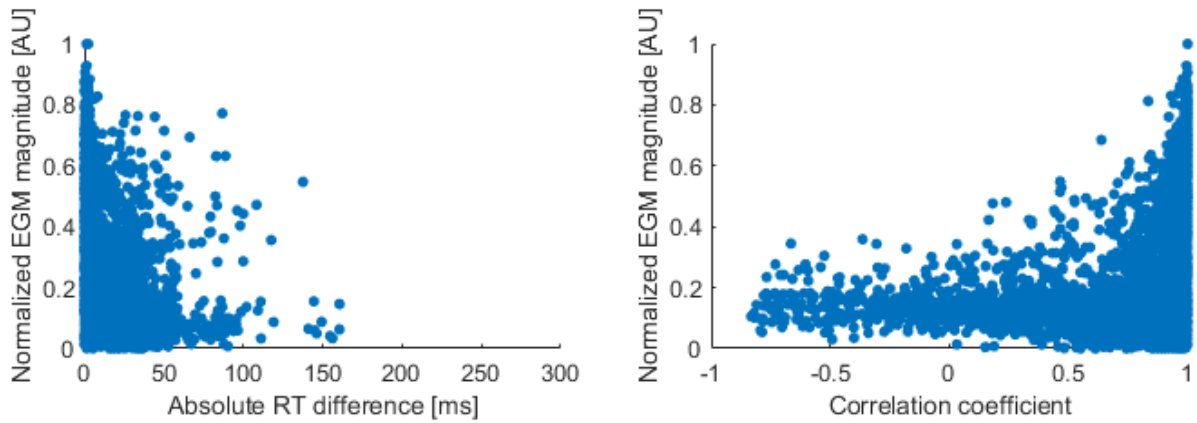


Figure 26: Normalized MUMC+ EGM magnitudes of the SR beats of patient 8 plotted against (Left) the absolute RT differences for the MUMC+-UMCU comparison of the SR beats of patient 8 (Right) the T-wave correlation coefficients for the MUMC+-UMCU comparison of the SR beats of patient 8.

Influence of noise on the RT difference and T-wave correlation

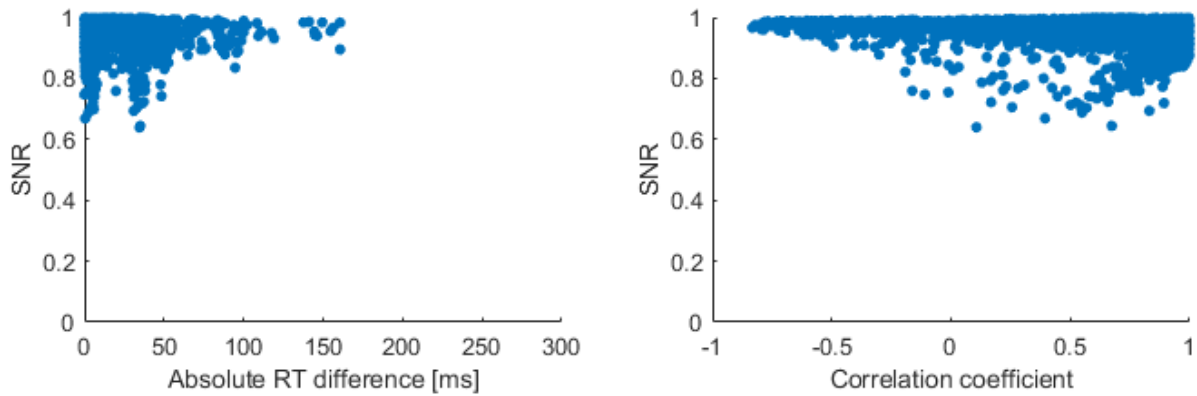


Figure 27: SNR of MUMC+ T-waves of the SR beats of patient 8 plotted against (Left) the absolute RT differences for the MUMC+-UMCU comparison of the SR beats of patient 8 (Right) the T-wave correlation coefficients for the MUMC+-UMCU comparison of the SR beats of patient 8.

4.2. Optimal set-up

4.2.1. Removal of electrodes

4.2.1.1. T-wave correlation

The median T-wave correlation coefficient for the reconstructions of the original UMCU set-up and the smaller UMCU set-ups (remove step 1 to 17) with the MUMC+ set-up reconstructions for SR beats and VES are shown in Figure 28. It is apparent from Figure 28 (solid black and red lines) that minor changes in the median correlation coefficient occur for most remove steps. By contrast, removal of inferior horizontal row of electrodes (remove step 17) showed a larger decrease in median correlation coefficient from the original UMCU-MUMC+ correlation in comparison to the other remove steps, for both SR beats and VES.

For both SR beats and VES, no decrease in median correlation coefficient was seen for separate removal of the strips consisting of three electrodes at the lateral sides of the thorax and the electrode strips posterior (Figure 28). For removal of some of these strips even slightly higher first quartiles were seen than for the UMCU-MUMC+ correlation coefficients. For the VES, the median correlation coefficient did also not change compared to the reference (UMCU-MUMC+) for the electrode strips consisting of five electrodes lateral/anterior (remove step 2 and 7), the strip of four electrodes at the left lateral side of the thorax (remove step 8) and for one strip consisting of seven electrodes at the right anterior side of the thorax (remove step 4). The information gathered with the electrodes at the positions of the mentioned vertical strips may therefore be of less additional value to the information already collected with the remaining electrodes.

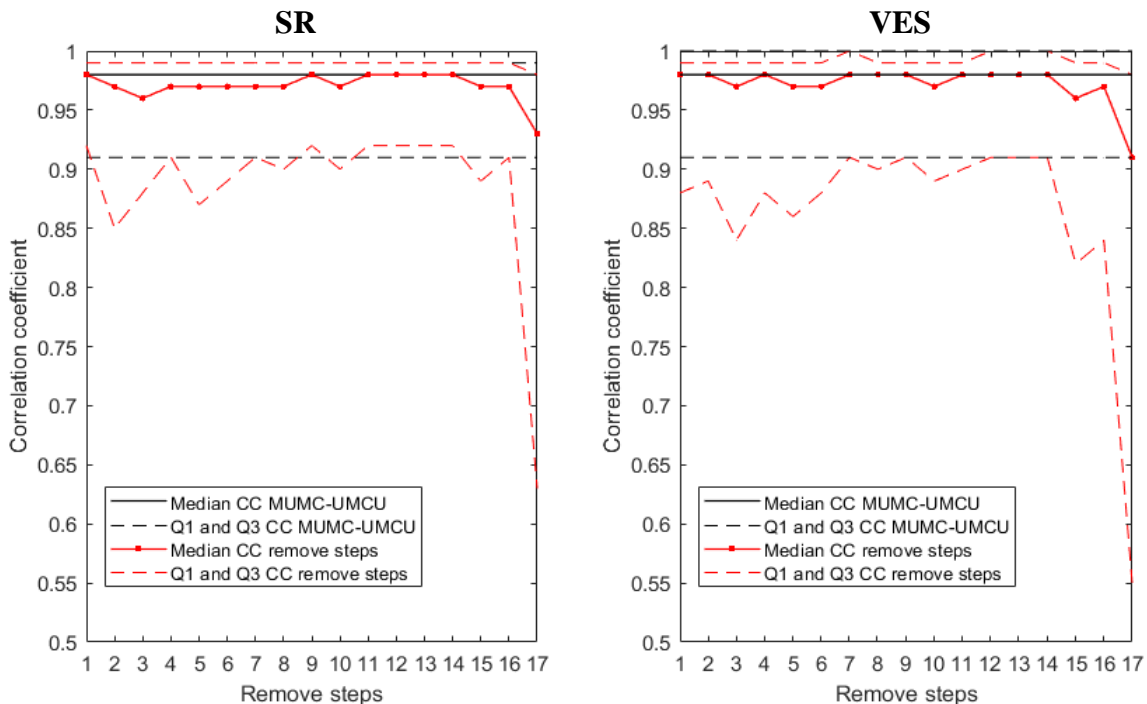


Figure 28: Median T-wave correlation coefficients with the first quartiles (lower dashed red line) and third quartiles (upper red dashed line) for the reconstructions of the smaller UMCU set-ups (remove step 1 to 17) with the MUMC+ set-up reconstructions for SR beats (left graph) and VES (right graph). The reference median T-wave correlation coefficient, first quartile and third quartile of the original UMCU set-up with the MUMC+ set-up reconstructions are shown in black.

4.2.1.2. Activation and recovery time

The median, first quartile and third quartile of the absolute AT differences for the UMCU-MUMC+ comparison and the smaller UMCU set-ups (remove step 1 to 17) reconstructions compared with the MUMC+ set-up reconstructions for SR beats and VES are shown in Figure 29. For the SR beats, separate removal of strips at the right lateral side (remove step 1, 2 and 14) did not deteriorate the AT difference. For the rest of the remove steps, the median absolute AT difference was increased to approximately 1 ms. Regarding the AT for VES, the left anterior vertical electrode strips (remove step 4 to 7) appear to be of less interest. In general, the left lateral/posterior vertical electrode strips, a strip of seven electrodes right anterior (remove step 3) and the upper, middle and lower horizontal strip of electrodes seem important for the AT of both SR beats and VES. Furthermore, removal of the strip consisting of five electrodes at the right anterior side (remove step 2) did not deteriorated the AT difference for both SR beats and VES.

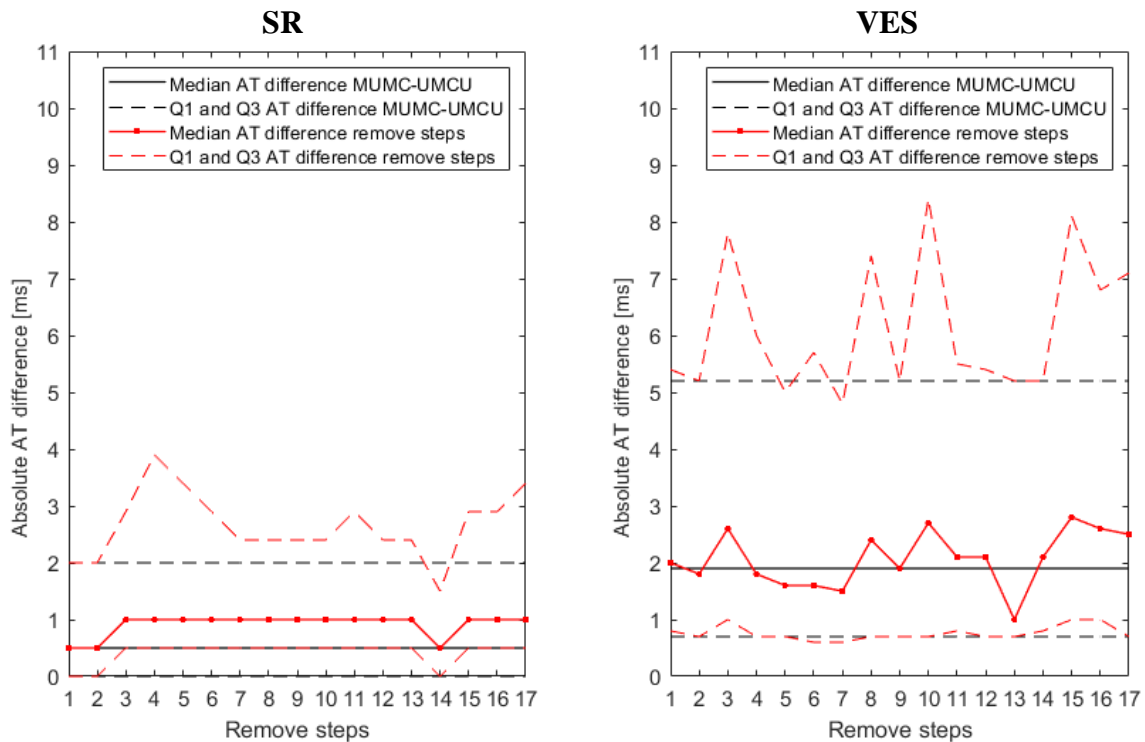


Figure 29: Median of node-to-node absolute AT differences with the first quartiles (lower dashed red line) and third quartiles (upper red dashed line) for the reconstructions of the smaller UMCU set-ups (remove step 1 to 17) with the MUMC+ set-up reconstructions for SR beats (left graph) and VES (right graph). The reference median absolute AT difference, first quartile and third quartile of the original UMCU set-up with the MUMC+ set-up reconstructions are shown in black.

The median, first quartile and third quartile of the absolute RT differences for the UMCU-MUMC+ comparison and the smaller UMCU set-ups (remove step 1 to 17) reconstructions compared with the MUMC+ set-up reconstructions for SR beats and VES are shown in Figure 30. In contrast to the results for the T-wave correlation (Figure 28), removal of the inferior horizontal strip of electrodes did not cause large changes in the RT difference for both SR beats and VES.

Small or even no change in RT difference was seen for removal of electrode strips at the right anterior/lateral/posterior side of the thorax and the inferior horizontal strip of electrodes. For SR, large increase in RT difference was seen if vertical strips left anterior were removed, if both left lateral strips were removed (remove step 10) and if the upper and middle horizontal strip of electrodes were removed. For VES, the median RT difference remained fairly the same for most remove steps.

Overall, the largest increases in RT difference were found for removal of the upper or middle horizontal strip of electrodes (remove step 15 and 16). The RT difference did not deteriorate for both SR beats and VES if the electrode strip consisting of five electrodes right anterior (remove step 2) was removed.

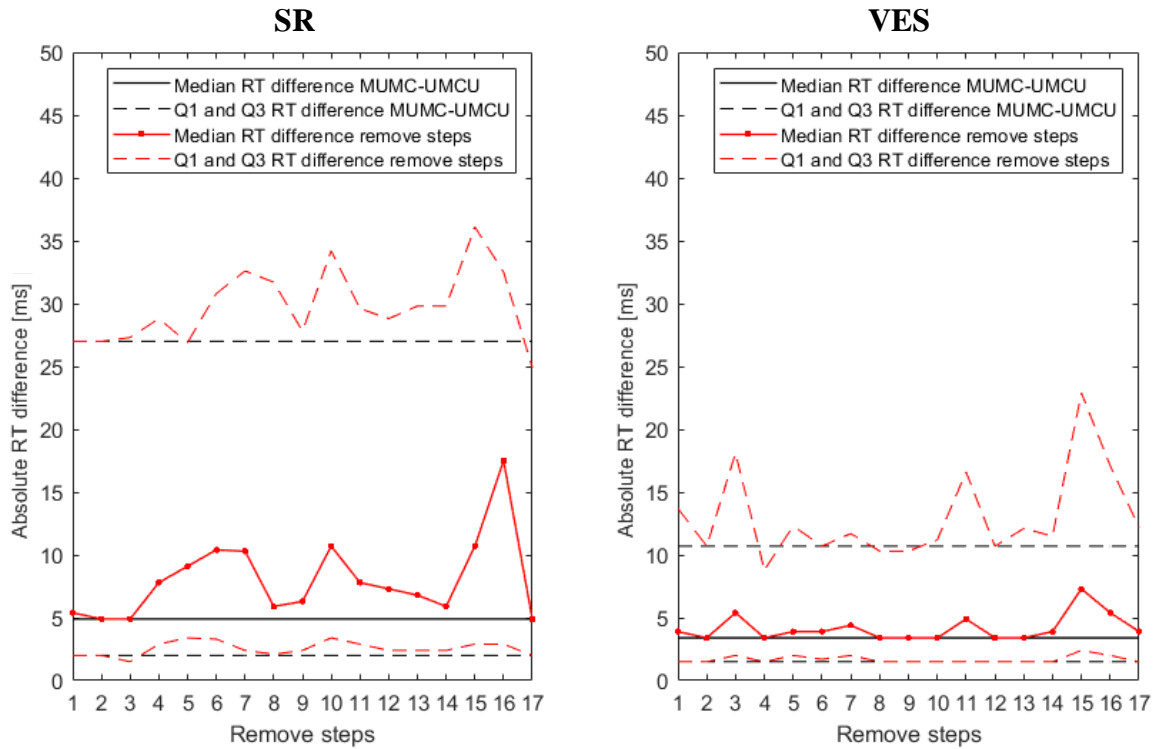


Figure 30: Median of node-to-node absolute RT differences with the first quartiles (lower dashed red line) and third quartiles (upper red dashed line) for the reconstructions of the smaller UMCU set-ups (remove step 1 to 17) with the MUMC+ set-up reconstructions for SR beats (left graph) and VES (right graph). The reference median absolute RT difference, first quartile and third quartile of the original UMCU set-up with the MUMC+ set-up reconstructions are shown in black.

Considering the T-wave correlation, AT differences and RT differences, removal of the horizontal rows of twelve electrodes seemed to have the largest impact. Furthermore, removal of the vertical rows of electrodes at the right lateral side and the posterior side of the thorax seemed of less interest to capture information additional to the information already gathered with other body-surface electrodes.

4.2.2. Addition of electrodes

4.2.2.1. T-wave correlation

Table 7 shows the median T-wave correlation coefficients of the UMCU set-up, the different enlarged UMCU set-ups (addition step 1 to 7) and the 100-electrodes set-up reconstructions relative to the MUMC+ reconstructions. For the addition of electrodes inferior (addition step 2), both inferior and superior (addition step 3) and at the lower left quadrant of the thorax (addition step 7), subtle increase in median correlation coefficient was seen in comparison to the original UMCU set-up. Focussing on the first and third quartile as shown in Table 7, the T-wave correlation also showed small improvement for the addition of electrodes only superior and at the upper left quadrant of the thorax. Overall, the largest improvement was seen for the addition of electrodes inferior. The addition of electrodes at the anterior right upper quadrant of the thorax (addition step 4) did not change the correlation. Furthermore, the addition of electrodes at the lower right quadrant (addition step 6) of the thorax showed slightly

decrease in median correlation coefficient for the SR beats. After further analysis, it turned out that for some of the reconstructions for addition step 6 rather small Tikhonov parameters were used in comparison to the MUMC+ reconstructions. For the VES, addition step 6 showed improvement in T-wave correlation. Furthermore, it can be seen in Table 1 that the correlation coefficients of the enlarged set-ups are reasonably close or equal to the T-wave correlation of the 100-electrodes set-up.

Table 7: Median T-wave correlation coefficients for SR beat and VES reconstructions of different electrode set-ups relative to MUMC+ reconstructions.

Median correlation coefficient T-wave (Q1 – Q3)	SR	VES
MUMC+ – UMCU	0.98 (0.91 – 0.99)	0.98 (0.91 – 1.00)
Addition step 1	0.98 (0.93 – 0.99)	0.98 (0.91 – 1.00)
Addition step 4	0.98 (0.91 – 0.99)	0.98 (0.91 – 1.00)
Addition step 5	0.98 (0.93 – 1.00)	0.98 (0.92 – 1.00)
MUMC+ – UMCU (M58 excluded)	0.98 (0.93 – 0.99)	0.98 (0.91 – 1.00)
Addition step 2 (M58 excluded)	0.99 (0.97 – 1.00)	0.99 (0.93 – 1.00)
Addition step 3 (M58 excluded)	0.99 (0.95 – 1.00)	0.99 (0.93 – 1.00)
Addition step 6 (M58 excluded)	0.97 (0.89 – 0.99)	0.99 (0.94 – 1.00)
Addition step 7 (M58 excluded)	0.99 (0.95 – 1.00)	0.99 (0.94 – 1.00)
100-electrodes set-up	0.99 (0.97 – 1.00)	0.99 (0.96 – 1.00)

4.2.2.2. Activation and recovery time

Table 8 shows the median absolute AT difference of the UMCU set-up, the different enlarged set-ups (addition step 1 to 7) and the 100-electrodes set-up reconstructions relative to the MUMC+ reconstructions. The addition of electrodes superior, inferior, both superior and inferior and at the lower left quadrant of the thorax (addition step 1, 2, 3 and 7) showed decrease in AT differences for both SR beats and VES. For the other addition steps, an increase in AT differences was seen for at least one of the beat types. It is apparent from Table 8 that the AT differences of the SR beats reconstructions of most the enlarged UMCU set-up were equal to the AT differences of the 100-electrodes set-up.

Table 8: Median of node-to-node absolute AT differences for SR beat and VES reconstructions of different electrode set-ups relative to MUMC+ reconstructions.

Median absolute AT difference [ms] (Q1 – Q3)	SR	VES
MUMC – UMCU	0.5 (0 – 2.0)	1.9 (0.7 – 5.2)
Addition step 1	0.5 (0 – 1.5)	1.7 (0.6 – 5.0)
Addition step 4	0.5 (0 – 1.5)	1.9 (0.8 – 5.3)
Addition step 5	0.5 (0 – 2.0)	2.1 (0.7 – 5.1)
MUMC – UMCU (M58 excluded)	0.5 (0 – 2.0)	1.9 (0.7 – 5.2)
Addition step 2 (M58 excluded)	0.5 (0 – 1.5)	1.7 (0.6 – 4.6)
Addition step 3 (M58 excluded)	0.5 (0 – 1.5)	1.4 (0.5 – 4.2)
Addition step 6 (M58 excluded)	1.0 (0.5 – 3.4)	2.2 (0.8 – 6.7)
Addition step 7 (M58 excluded)	0.5 (0 – 1.5)	1.7 (0.6 – 4.5)
100-electrodes set-up	0.5 (0 – 1.5)	0.6 (0.3 – 2.2)

The median absolute RT difference of the UMCU set-up, the different enlarged UMCU set-ups (addition step 1 to 7) and the 100-electrodes set-up reconstructions relative to the MUMC+ reconstructions are shown in Table 9. For both SR beats and VES, the addition of electrodes inferior, both inferior and superior and at the upper and lower left quadrant of the thorax (addition step 2, 3, 5 and 7) showed decrease in RT differences. For the other addition steps, an increase in RT differences was seen for at least one of the beat types. Although the RT differences decreased for some of the enlarged set-ups, the RT differences were still smaller for the 100-electrodes set-up.

Table 9: Median of node-to-node absolute RT differences for SR beats and VES reconstructions for different electrode set-ups relative to MUMC+ reconstructions.

Median absolute RT difference [ms] (Q1 – Q3)	SR	VES
MUMC – UMCU	4.9 (2.0 – 26.9)	3.4 (1.5 – 10.7)
Addition step 1	4.7 (1.5 – 27.9)	3.9 (1.5 – 11.2)
Addition step 4	5.0 (2.0 – 27.1)	3.4 (1.5 – 10.7)
Addition step 5	3.9 (2.0 – 25.4)	2.9 (1.5 – 8.8)
MUMC – UMCU (M58 excluded)	4.9 (2.0 – 26.9)	3.4 (1.5 – 10.7)
Addition step 2 (M58 excluded)	4.4 (1.5 – 24.9)	2.9 (1.5 – 8.8)
Addition step 3 (M58 excluded)	3.9 (1.5 – 25.4)	2.9 (1.5 – 9.3)
Addition step 6 (M58 excluded)	16.6 (3.9 – 39.6)	4.4 (2.0 – 15.1)
Addition step 7 (M58 excluded)	4.4 (2.0 – 21.0)	2.9 (1.5 – 9.3)
100-electrodes set-up	2.9 (1.0 – 20.0)	1.5 (0.5 – 3.6)

Considering the T-wave correlation, absolute AT differences and absolute RT differences, the inferior area and lower left area of the thorax seemed of interest to capture additional information.

4.2.3. Optimal set-up

Overall, the body-surface electrodes at the right lateral side and the posterior side of the thorax seemed of less value for the correct reconstruction of the T-wave and correct determination of AT and RT (Figure 31). These vertical electrode rows consisted of three to five electrodes. Based on the removal and addition of electrodes, the areas of the horizontal rows, consisting of 12 electrodes, and the anterior vertical electrode strips, consisting of five or seven electrodes, seemed most important (Figure 31).

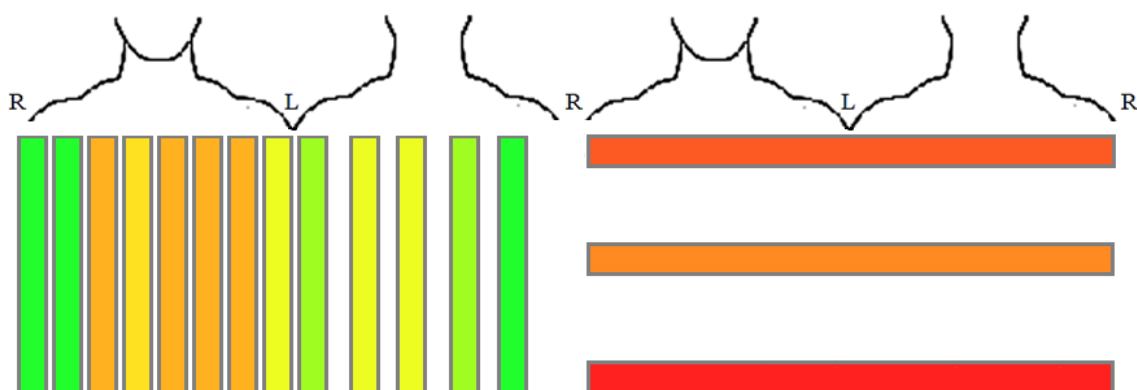


Figure 31: Schematic representation of the UMCU set-up on a torso in vertical and horizontal strips. The colour indicates the extent to which the area of the strip is important; red is important and green is less important.

4.2.3.1. Minimizing the number of electrodes

Table 10 shows the T-wave correlation, median absolute AT and median absolute RT differences for three set-ups, consisting of 51, 45 and 37 electrodes. For the set-up of 51 electrodes, the vertical rows of electrodes for remove step 2, 9 and 13 were all removed. For the set-up of 45 electrodes, also the electrodes for remove step 1 and 14 were removed. The set-up consisting of 37 electrodes was created by also removing the electrodes of remove step 11 and 12, and therefore did not contain electrodes posterior of the thorax.

As can be seen in Table 10, the results of the 51-electrodes set-up and 45-electrodes set-up were reasonably in line with the results of the UMCU set-up. For the SR beats, slightly larger absolute AT and RT differences were found for the 51-electrodes and 45-electrodes set-up in comparison to the UMCU set-up. In contrast to the VES reconstructions, in which smaller AT and RT differences were found for the 51-electrodes and 45-electrodes set-up in comparison to the UMCU set-up. The 37-electrodes set-up showed overall deterioration, with for example a substantial reduction in first quartile of the T-wave correlation and a doubling of the median RT difference for SR beats.

Table 10: Median T-wave correlation, median of node-to-node absolute AT differences and median of node-to-node absolute RT differences for SR beats and VES reconstructions for different electrode set-ups relative to MUMC+ reconstructions.

	SR	VES
Median T-wave correlation (Q1 – Q3)		
64 electrodes (UMCU)	0.98 (0.91 - 0.99)	0.98 (0.91 - 1.00)
51 electrodes (remove step 2, 9 & 13)	0.97 (0.90 - 0.99)	0.98 (0.86 - 0.99)
45 electrodes (remove step 1, 2, 9, 13 & 14)	0.97 (0.86 - 0.99)	0.97 (0.82 - 0.99)
37 electrodes (remove step 1, 2, 9, 11, 12, 13 & 14)	0.94 (0.61 - 0.99)	0.95 (0.66 - 0.99)
Median absolute AT difference [ms] (Q1 – Q3)		
64 electrodes (UMCU)	0.5 (0 - 2.0)	1.9 (0.7 - 5.2)
51 electrodes (remove step 2, 9 & 13)	1.0 (0.5 - 2.4)	1.4 (0.6 - 4.4)
45 electrodes (remove step 1, 2, 9, 13 & 14)	1.0 (0.5 - 2.4)	1.6 (0.6 - 4.7)
37 electrodes (remove step 1, 2, 9, 11, 12, 13 & 14)	1.0 (0.5 - 5.9)	2.5 (0.9 - 9.1)
Median absolute RT difference [ms] (Q1 – Q3)		
64 electrodes (UMCU)	4.9 (2.0 - 27.0)	3.4 (1.5 - 10.7)
51 electrodes (remove step 2, 9 & 13)	6.6 (2.4 - 29.8)	2.4 (1.0 - 6.8)
45 electrodes (remove step 1, 2, 9, 13 & 14)	7.8 (2.4 - 30.7)	2.4 (1.0 - 7.3)
37 electrodes (remove step 1, 2, 9, 11, 12, 13 & 14)	11.2 (2.9 - 31.7)	3.9 (1.5 - 16.6)

4.2.3.2. Adjusted 64-electrodes set-up

It was investigated whether the 64 electrodes of the UMCU set-up provided better agreement with the MUMC+ set-up if the electrodes were placed in other positions around the thorax. For this purpose, the electrodes of remove step 2, 9 and 13 (13 electrodes in total) were placed inferior of the original UMCU set-up at the positions of addition step 2 (10 electrodes) and at the lower left anterior quadrant at the positions of addition step 7 (3 electrodes). Table 11 shows the median T-wave correlation, median AT difference and median RT difference of the original UMCU set-up and the adjusted 64-electrodes set-up. As can be depicted from Table 11, for the median T-wave correlation no change was observed. For the AT and RT differences zero or minor improvements were seen for the adjusted 64-electrodes set-up in comparison to the original UMCU set-up.

Table 11: Median T-wave correlation, median of node-to-node absolute AT differences and median of node-to-node absolute RT differences for SR beats and VES reconstructions of the original UMCU set-up and an adjusted 64-electrodes set-up, relative to MUMC+ reconstructions.

	Median T-wave correlation (Q1 – Q3)		Median absolute AT difference [ms] (Q1 – Q3)		Median absolute RT difference [ms] (Q1 – Q3)	
	SR	VES	SR	VES	SR	VES
Original UMCU set-up	0.98 (0.93 – 0.99)	0.98 (0.91 – 1.00)	0.5 (0 - 2.0)	1.9 (0.7 - 5.2)	4.9 (2.0 – 26.9)	3.4 (1.5 – 10.7)
Adjusted 64-electrodes set-up	0.98 (0.93 - 0.99)	0.98 (0.91 – 1.00)	0.5 (0 - 1.5)	1.4 (0.5 – 4.0)	4.9 (2.0 - 27.3)	2.4 (1.0 - 6.8)

5. Discussion

The objective of this study was to assess how the body-surface potential measurements should be performed in terms of electrode number and distribution for high quality ECGI regarding the assessment of regional repolarization differences.

First, the ECGI quality of current used electrode set-ups was investigated. The results suggest reasonably high ECGI quality for the UMCU and Amsterdam UMC set-up. These results are supported by a recent published study of Gharbalchi No et al.⁵⁷ They simulated 192 body-surface potentials from 490 measured epicardial potentials with the use of a forward model. With the use of an algorithm, reduced leadsets of 64 and 32 electrodes were determined. They compared the inverse reconstructions of the set-ups and state that the 64-electrodes set-up performs as well as the 192-electrodes set-up.⁵⁷

In order to properly interpret the results, the interpretation of the outcome measures should be clarified. Pearson's correlation coefficients above 0.8 are generally considered high.⁵⁸ If the Pearson's correlation coefficient is one, the T-waves for the compared node of two inverse reconstructions correspond perfectly. For most patients, the median correlation coefficients of the UMCU and Amsterdam UMC reconstructions with the MUMC+ reconstructions approached one. Furthermore, the first quartiles were almost always above 0.8. In contrast to the standard 9-electrodes reconstructions for which the median correlation coefficients with the MUMC+ reconstructions were lower than 0.8 in some patients and considerably low first quartiles were found.

For interpretation of AT and RT differences, it is important to take some factors into account. As mentioned, larger differences were expected for RT in comparison to AT considering the lower voltage and longer duration of the T-wave in comparison to the QRS complex. Because of the lower slope of the T-wave, noise has larger influence on the determination of the RT point than the AT point. Furthermore, it is of value to know the lengths of the selected QRS and T-wave segments, in which the AT or RT points were determined. For the used data, the QRS segments and T-wave segments for SR beats were approximately 120 ms and 260 ms, respectively. For the VES, the QRS segments were approximately 160 ms and the T-wave segments approximately 300 ms. Focussing on the results, for a large portion of nodes for the UMCU and Amsterdam UMC reconstructions the AT and RT differences with the MUMC+ reconstructions were very small (median AT difference between 0.5 – 1.9 ms and median RT difference between 2.9 – 7.3 ms), considering the length of the segments. Therefore, the AT and RT maps of the UMCU and Amsterdam UMC set-up had overall good agreement with the MUMC+ set-up maps. For the standard 9-electrodes reconstructions a wider range of frequent AT and RT differences with the MUMC+ reconstructions was present (Figure 16), which indicates that the standard 9-electrodes maps of AT and RT over the epicardium can differ considerably from the MUMC+ set-up maps. However, all three set-ups showed outliers in AT and RT. So, regardless of the number of electrodes, epicardial regions with differences were present. Further exploration of the RT differences between the reconstructions of the different set-ups showed that (a portion of) the larger RT differences can be explained by the electrogram magnitude and T-wave amplitude (Figure 25 and 26). Flat T-waves are a known difficulty for correct RT point determination and result in lower T-wave correlation coefficients. Therefore, differences between the used outcome measures will simply exist for electrode set-ups with different number or distribution of electrodes. As mentioned, the concept of ECGI is to determine a physiological solution for epicardial electrograms which best describes the measured body-surface potentials. Possibly, epicardial areas with low reconstructed potential amplitudes are of less influence on the solution choice, what could lead to totally different electrograms for these areas with only a slightly different composition of body-surface potentials.

The two outcome measures “activation duration” and “recovery duration” were created to have node-to-node independent outcome measures and therefore exclude the effect of a possible spatial shift of the reconstruction. Overall, the UMCU reconstructions and Amsterdam UMC reconstructions resulted in smaller differences in activation duration and recovery duration with the MUMC+ reconstructions in comparison to the standard 9-electrodes reconstructions. However, it was also seen that these two outcome measures fluctuate for different patients. Sometimes, the activation duration and recovery duration differences for the UMCU and Amsterdam UMC reconstructions were even higher than for the standard 9-electrodes reconstructions. These fluctuations can be caused by the way these

two outcome measures were determined. The outcome measures were determined as the difference between the mean of five earliest ATs or RTs and the mean of the five latest ATs and RTs. If outliers are present in the earliest or latest five ATs or RTs, the mean can differ greatly. Because of the fluctuations per patient, it is difficult to draw a conclusion whether the activation and recovery durations are sufficiently similar with the reconstructions of the MUMC+ set-up.

Regarding the repolarization gradients, between the UMCU and Amsterdam UMC reconstructions and the MUMC+ reconstructions, also overall smaller differences were seen than between the standard 9-electrodes and MUMC+ reconstructions. Furthermore, visually better agreement was seen for the UMCU and Amsterdam UMC reconstructions than for the standard 9-electrodes reconstruction with the MUMC+ reconstructions. However, as for the activation and recovery duration, the difference in 95th percentile of the gradients fluctuated between the patients. Different gradients were present between the patients, for example in some patients gradients of 350 ms/cm were present, while in other patients the gradients were around 180 ms/cm. Unpublished research at the MUMC+ also showed fluctuations in gradients in control patients. Greater fluctuations between the control patients were seen for the maximal gradient than for the 95th percentile of the gradients. For this reason the 95th was used as outcome measure to compare the repolarization gradients. In this study the larger differences in 95th percentile of the gradients were not necessarily found in the patients with the higher gradients. Because both large and small differences in gradients were found, the number of electrodes does not necessarily seem the only cause of the differences. At this point, it is difficult to make a statement about whether the gradients of the investigated set-ups correspond well enough with the MUMC+ set-up. The differences may also be related to the way the gradients were calculated. For example, it is important that the RTs are determined correctly, because the gradients are calculated from the RTs. Furthermore, it is not yet decided within the VIGILANCE study how the gradients should be evaluated. This should be set first, in order to correctly interpret if these differences are clinically (un)acceptable.

In this study, the influence of EGM magnitude, T-wave amplitude and noise in the T-wave segment on the RT determination and T-wave correlation were investigated. In general, larger RT differences and lower T-wave correlation coefficients were found for lower EGM magnitude and lower T-wave amplitude. Because lower correlation coefficients were already expected for flat T-waves, T-waves defined as flat (with the method in this study) were excluded from the T-wave correlation calculation. However, it was found that only a minority of low amplitude T-waves, which resulted in low T-wave correlation coefficients, were removed. As can be seen in Figure 25 (right graph), many low amplitude T-waves resulted in low correlation coefficients. However, for the same low T-wave amplitudes also high T-wave correlation coefficients were found. Therefore, no clear amplitude limit can be extracted from the results. A possible explanation is the normalization of the T-wave amplitude. The T-wave amplitudes were normalized within their local EGM. But, in low magnitude EGMs, noise is more prevalent than in EGMs with higher magnitude. However, the results did not show a trend between noise in the T-wave segment and the RT difference or the T-wave correlation (Figure 27).

Overall, slightly better results were seen for the UMCU set-up in comparison to the Amsterdam UMC set-up. The main difference between the UMCU set-up and Amsterdam UMC set-up is the electrode distribution. In the UMCU set-up, the electrodes are more evenly distributed, while the Amsterdam UMC set-up is non-uniform (highest density of electrodes on the lower left anterior side) and has more electrodes posterior than the UMCU set-up.

Next, the number and positioning of the body-surface electrodes necessary for high quality ECGI were investigated. The results indicate that a reduced electrode set-up consisting of 51 electrodes can have good agreement with the MUMC+ set-up regarding the T-wave correlation, AT and RT, with the electrode positions carefully chosen (Table 10). Furthermore, the investigated set-up consisting of 45 electrodes seems sufficient. For the set-up stated in Table 10 consisting of 37 electrodes, the reconstruction differences became larger and is therefore suggested insufficient.

The importance of the electrode position is visible in Figure 28, 29 and 30. For example, an electrode set-up consisting of 52 electrodes, due to removal of the lowest 12 electrodes of the UMCU set-up, showed considerable decrease in T-wave correlation in comparison to the other 52-electrodes set-ups. This set-up (remove step 17) showed worse T-wave correlation than the 37-electrodes set-up of Table 10. The results show which electrode positions seem to provide important information. Overall, the electrodes at the right lateral side and the posterior side of the thorax seem to be less important for

correct inverse reconstruction (Figure 31). This finding was also observed for BSPM. Finlay et al.⁵⁹ found that set-ups with electrodes only at the posterior and lateral regions of the thorax performed less favourably for BSPM than those set-ups where electrodes could also be chosen at the anterior side of the thorax. The vertical row of five electrodes at the right anterior side of the thorax (remove step 2) seems least important. For correct T-wave reconstruction and AT determination, the lowest horizontal row of electrodes seems to be of value. For correct AT determination of VES, also the upper and middle horizontal row of electrodes (remove step 15 & 16) seem to be important. In addition, the vertical row of four electrodes on the left lateral-anterior side of the thorax (remove step 8) and the horizontal row of seven electrodes on the right anterior side of the thorax (remove step 3) seem to be of value. For correct RT determination also the upper and middle horizontal row of electrodes of the original UMCU set-up seem to be important. Furthermore, the left anterior vertical rows of electrodes are important for correct RT determination of SR beats.

The addition of electrodes to the UMCU set-up provided insight in electrode positions of interest to capture additional information. The largest improvement was seen for the addition of a horizontal row of ten electrodes inferior to the original UMCU set-up. Furthermore, the lower left anterior quadrant of the thorax seems to be important. The importance of these electrode locations seems reasonable, given the anatomical location of the heart and the direction of the heart axis for SR beats. In literature, the body-surface electrode locations centred over the heart also showed to contain relevant data for the inverse reconstruction.⁶⁰ For both removal and addition of inferior electrodes, change in the outcome measures was observed, which emphasizes the importance of these electrode positions. This finding is contrary to the study of Jiang et al.⁶¹, who found that the electrodes located on the lower part of the thorax are redundant. However, the study of Jiang et al. was based on a model and focussed on the optimization of electrode positions for the reconstruction of ischemic areas. The study was therefore focussed on an optimal set-up for maximum diagnostic information of ischemic areas instead of maximum signal information. Furthermore, the results of the enlarged UMCU set-ups were compared to the results of a 100-electrodes set-up (Table 7, 8 and 9). The T-wave correlation and AT differences of some enlarged set-ups were quite similar to those of the 100 electrode set-up. In addition, the results of the 100-electrodes set-up showed that also for these reconstructions larger regional RT differences with the MUMC+ reconstructions existed.

Finally, it was investigated whether the reconstructions for a different distribution of 64 electrodes resulted in better agreement with the MUMC+ reconstructions than the current distribution of the UMCU set-up. Despite the fact that for this set-up the electrodes at the locations of least importance were moved to locations that improved the inverse reconstruction, only minor or zero improvement in outcome measures was seen for the adjusted set-up. This indicates that the original UMCU set-up was already reasonably optimal for 64 electrodes. This statement is supported by Donnelly et al.¹⁹, who stated that for BSPM many “near-optimal” solutions exist for any number of recording sites, which perform comparably with insignificant differences.

5.1. Ground truth

The results should be interpreted in view of the limitations of this study. It should be noted that the true ground truth for the reconstructed EGMs of the inverse reconstructions are measured EGMs at the patients' epicardium. For this study the 184-electrodes set-up was assumed to provide sufficient ECGI quality and was therefore used as ground truth. The MUMC+ set-up as ground truth provides an impression on the inverse reconstructions for different body-surface electrode set-ups, without the need of invasive measurements. Because of this, however, it could not be investigated if a set-up of less than 184 electrodes can be more sufficient for ECGI than the 184-electrodes set-up.

5.2. Electrode set-ups

The number of electrodes of the MUMC+ set-ups were not all equal to 184 for the different patients and different beats. This is due to exclusion of inadequate electrodes for the inverse reconstruction.

Moreover, the MUMC+ set-up is not standardized. This contributed to the fact that the correct locations for electrodes of the selected set-ups could not always be found. Furthermore, the addition of electrodes was therefore focussed on regions on the thorax and not on specific locations. It was decided to keep the number of electrodes for the selection of the UMCU, Amsterdam UMC and standard 9-electrodes set-up equal to its originals (i.e. inadequate electrodes had to be exchanged for adequate electrodes at other locations). Overall, this created differences between the selected set-ups for the different patients. Furthermore, if the MUMC+ set-up had been standardized, electrode placement could be examined more specifically.

It is also important to evaluate the practicality and (dis)advantages of the electrode systems. The MUMC+ set-up consists of fixed electrode strips. Because of this, good contact of electrodes with the body depends on the curves of the body. For example, due to breasts, electrodes centred over the heart may be lost. However, strips allow quick placement of a large number of electrodes on the thorax. On the other hand, preparation and cleaning of these electrode strips is time-consuming, which limits the clinical usability. The system is still mainly used for research purposes. The UMCU normally makes use of a system consisting of separate disposable electrodes, requiring no preparation and cleaning of the electrodes. Furthermore, the disposable electrodes can also be applied reasonably fast to the body surface. A lower number of electrodes necessary for ECGI can improve the practicality of the electrode systems.

5.3. Inverse reconstruction

Also some inverse reconstruction related topics should be discussed. First, the transfer matrix was calculated based on all electrodes of the MUMC+ set-up, to exclude the effect of the transfer matrix for this simulated inter-system comparison. However, in the participating hospitals of the VIGILANCE study the transfer matrix is currently calculated based on the number of electrodes of the set-up. A lower number of electrodes can therefore lead to a less detailed torso geometry for the transfer matrix calculation. For future application of reduced lead set-ups for ECGI, the use of a more detailed body-surface geometry obtained from the geometry information in the CT or MRI scan could be considered.

Second, the Tikhonov parameter choice plays an important role in the occurrence of differences between inverse reconstructions. For example, for the Amsterdam UMC reconstructions of patient 6, substantial differences with the MUMC+ reconstructions were observed due to the used Tikhonov parameter. For this study, the Tikhonov parameter was determined per selected set-up and was therefore based on the balance between the available information of the selected electrodes and the need for regularization. For one patient a fairly lower Tikhonov parameter was chosen by the regularization method for the reconstruction for an electrode set-up of 69 electrodes (addition step 6) in comparison to the UMCU 64-electrodes set-up. The resulting reconstructions of the 69-electrodes set-up differed more with the MUMC+ reconstructions than the UMCU reconstructions, while basically more information was available. On which basis the Tikhonov parameter for certain electrode set-ups is chosen in comparison to the available information of other set-ups needs further investigation.

This study concerns a very useful topic for the reliability of ECGI. It is important to keep in mind the robustness of ECGI. Because the inverse problem is ill-posed, small changes in the BSPs are amplified in the solution. In ECGI, regularization is applied to improve the robustness of the inverse solution. In addition, electrodes with excessive noise (e.g. due to contact loss) are removed and the remaining BSPs are filtered for all kinds of noise. However, with decreasing number of body-surface electrodes, it becomes more important that the electrodes do not contain excessive noise, as those electrodes will be excluded for the inverse reconstruction. But, as earlier mentioned, it is more controllable with smaller numbers of electrodes. This study showed that the Tikhonov parameter can differ considerably with only a small change in the composition of the included BSPs, causing substantial changes between reconstructions. Insight into the Tikhonov parameter choice is therefore necessary for further assessing the robustness of ECGI to noise.

5.4. Outcome measures

This research revealed some difficulties of the used outcome measures. For example, it is currently difficult to compare repolarization gradients. For the VIGILANCE study, it is important to further examine how the gradients should be evaluated. Furthermore, this study revealed AT and RT artefacts for the used ECGI method. In addition, the presented method to calculate activation duration and recovery duration showed to be sensitive to these AT and RT artefacts. Normally, the ATs and RTs are determined relative to the earliest epicardial AT. If this earliest epicardial AT is an artefact, this error is propagated to the calculated ATs and RTs. It might be beneficial to look at several early AT points and take the average of them, for example.

The occurrence of RT artefacts stands out. A possible cause for the RT artefacts is broad selection of the T-wave segment. Furthermore, the use of the spatiotemporal method seems to play a role in the arise of RT artefacts. Bear et al.⁶² described RT artefacts due to the use of the spatiotemporal method as unsurprising, as the method is based on a spatial connection, which does not necessarily exist in repolarization. To identify and remove RT artefacts, post-processing of the RTs was implemented. In this study, the uncertainty score was developed for the detection of RTs which seem uncertain based on the temporal expectation. However, not all RT artefacts were classified as uncertain with the used uncertainty score. As can be seen in Figure 16, it remains difficult for flat T-waves. Figure 16 shows that the RT point for the UMCU set-up is set in the steepest upslope in the T-wave segment and is therefore assessed as certain. Other post-processing options were considered. For example, only include RTs between the 2nd and 98th percentile. However, for this option, the excluded RTs consisted of many certain RTs. It would be optimal if the correctness of the RT does not have to be assessed afterwards, but that a check has already been implemented in the determination, so that fewer incorrect RTs arise initially. The used method for RT determination is sensitive to noise. It may therefore be beneficial to look at other solutions for RT determination. For example, incorporating the uncertainty score in the determination, so that RTs can only be determined within the largest positive area of the derivative.

5.5. Future perspectives

Soon, an open-source algorithm called UNISYS becomes available, which provides a unified graphical bullseye representation of cardiac ventricular data, whilst considering inter-individual anatomical aspects.⁶³ This algorithm can be used to provide insight in the specific epicardial regions of reconstruction differences. In addition to the outcome measures used in this study, it is interesting to compare the ECGI quality of different electrode set-ups based on localization of VES origin.

Furthermore, this study highlights ECGI related issues, which require further investigation. Among other things, improvement of the RT determination must be considered. In addition, it is interesting to investigate on which aspects of the body-surface potentials the lower Tikhonov parameter choices were based for some of the reconstructions. Furthermore, the newly developed uncertainty score should be validated.

Other methods could be useful to investigate more specifically the value of body-surface electrode locations and the necessary number of electrodes. For example, an algorithm can be developed, which automatically searches for an optimal set-up regarding the distribution of a minimal number of electrodes for which the reconstruction accuracy is still considered sufficient. Due to the time required for each inverse reconstruction, such an algorithm is very time-consuming. In addition, interpolation of electrodes on the chest could be considered, in order to require a lower number of electrodes actually placed on the chest. However, the study of Bear et al.⁶⁰ showed no improvement of reconstruction accuracy for linear interpolation of lost BSPs.

At last, the value of ECGI in IVF is still to be investigated in the VIGILANCE project. For this, it is important to establish when repolarization gradients can be considered physiological and pathological.

6. Conclusion

The findings support the hypothesis that the 64-electrodes UMCU set-up and 62-electrodes Amsterdam UMC set-up is sufficient and the standard 9-electrodes set-up is insufficient for use in ECGI. Furthermore, in this study a lower limit of number of electrodes, necessary for sufficient ECGI quality regarding the assessment of repolarization, was found around 45 electrodes. The electrodes at the right lateral side and posterior side of the thorax proved of less value for the inverse reconstruction. Separate removal of the upper, middle and lower horizontal row of 12 electrodes of the UMCU set-up generally had the largest effect on the investigated outcome measures. The lower row of electrodes again proved important when investigating the addition of electrodes. Furthermore, it is important to have enough electrodes on the lower left quadrant of the thorax.

This study increases our understanding of the effect of electrode number and placement on the inverse reconstruction. A simulated inter-system comparison was performed, keeping many aspects of ECGI unchanged. Furthermore, this study uncovered current difficulties of ECGI, such as recovery time determination, which is important for interpretation of inverse reconstructions. In addition, the uncertainty score was developed for the detection of uncertain recovery times, which is of added value for ECGI.

7. References

1. Wong CX, Brown A, Lau DH, et al. Epidemiology of Sudden Cardiac Death: Global and Regional Perspectives. *Hear Lung Circ.* 2019;28(1):6-14. doi:10.1016/j.hlc.2018.08.026.
2. Gräsner J-T, Lefering R, Koster RW, et al. EuReCa ONE-27 Nations, ONE Europe, ONE Registry: A prospective one month analysis of out-of-hospital cardiac arrest outcomes in 27 countries in Europe. *Resuscitation.* 2016;105:188-195. doi:10.1016/j.resuscitation.2016.06.004.
3. Fishman GI, Chugh SS, DiMarco JP, et al. Sudden Cardiac Death Prediction and Prevention Report From a National Heart, Lung, and Blood Institute and Heart Rhythm Society Workshop. *Circulation.* 2010;122(22):2335-2348. doi:10.1161/CIRCULATIONAHA.110.976092.
4. Waldmann V, Bougouin W, Karam N, et al. Characteristics and clinical assessment of unexplained sudden cardiac arrest in the real-world setting: focus on idiopathic ventricular fibrillation. *Eur Heart J.* 2018;39(21):1981-1987. doi:10.1093/eurheartj/ehy098.
5. Zipes DP, Camm AJ, Borggrefe M, et al. ACC/AHA/ESC 2006 guidelines for management of patients with ventricular arrhythmias and the prevention of sudden cardiac death: a report of the American College of Cardiology/American Heart Association Task Force and the European Society of Cardiology Com. *J Am Coll Cardiol.* 2006;48(5):e247-e346. doi:10.1016/j.jacc.2006.07.010.
6. Priori SG, Wilde AA, Horie M, et al. HRS/EHRA/APHRS expert consensus statement on the diagnosis and management of patients with inherited primary arrhythmia syndromes: document endorsed by HRS, EHRA, and APHRS in May 2013 and by ACCF, AHA, PACES, and AEPC in June 2013. *Hear Rhythm.* 2013;10(12):1932-1963. doi:10.1016/j.hrthm.2013.05.014.
7. Ozaydin M, Moazzami K, Kalantarian S, Lee H, Mansour M, Ruskin JN. Long-Term Outcome of Patients With Idiopathic Ventricular Fibrillation: A Meta-Analysis. *J Cardiovasc Electrophysiol.* 2015;26(10):1095-1104. doi:10.1111/jce.12737.
8. Blom LJ, Visser M, Christiaans I, et al. Incidence and predictors of implantable cardioverter-defibrillator therapy and its complications in idiopathic ventricular fibrillation patients. *EP Eur.* 2019;21(10):1519-1526. doi:10.1093/europace/euz151.
9. Meijborg VMF, Conrath CE, Opthof T, Belterman CNW, de Bakker JMT, Coronel R. Electrocardiographic T Wave and its Relation With Ventricular Repolarization Along Major Anatomical Axes. *Circ Arrhythmia Electrophysiol.* 2014;7(3):524-531. doi:10.1161/CIRCEP.113.001622.
10. Zhang J, Hocini M, Strom M, et al. The Electrophysiological Substrate of Early Repolarization Syndrome: Noninvasive Mapping in Patients. *JACC Clin Electrophysiol.* 2017;3(8):894-904. doi:10.1016/j.jacep.2016.12.017.
11. Antzelevitch C, Burashnikov A. Overview of Basic Mechanisms of Cardiac Arrhythmia. *Card Electrophysiol Clin.* 2011;3(1):23-45. doi:10.1016/j.ccep.2010.10.012.
12. Node T, Shimizu W, Taguchi A, et al. Malignant Entity of Idiopathic Ventricular Fibrillation and Polymorphic Ventricular Tachycardia Initiated by Premature Extrasystoles Originating From the Right Ventricular Outflow Tract. *J Am Coll Cardiol.* 2005;46(7):1288-1294. doi:10.1016/j.jacc.2005.05.077.
13. Cluitmans MJM, Peeters RLM, Westra RL, Volders PGA. Noninvasive reconstruction of cardiac electrical activity: update on current methods, applications and challenges. *Netherlands Hear J.* 2015;23(6):301-311. doi:10.1007/s12471-015-0690-9.
14. Blom LJ, Volders PGA, Wilde AA, Hassink RJ. Life-long tailoring of diagnosis and management of patients with idiopathic ventricular fibrillation - future perspectives in research. *Netherlands Hear J.* 2018;26(7-8):367-374. doi:10.1007/s12471-018-1123-3.
15. Oostendorp TF, van Dessel PFHM, Coronel R, et al. Noninvasive detection of epicardial and endocardial

- activity of the heart. *Netherlands Hear J*. 2011;19(11):488-491. doi:10.1007/s12471-011-0206-1.
16. Zhang J, Sacher F, Hoffmayer K, et al. Cardiac Electrophysiological Substrate Underlying the ECG Phenotype and Electrogram Abnormalities in Brugada Syndrome Patients. *Circulation*. 2015;131(22):1950-1959. doi:10.1161/CIRCULATIONAHA.114.013698.
 17. Vijayakumar R, Silva JNA, Desouza KA, et al. Electrophysiologic Substrate in Congenital Long QT Syndrome: Noninvasive Mapping with Electrocardiographic Imaging (ECGI). *Circulation*. 2014;130(22):1936-1943. doi:10.1161/CIRCULATIONAHA.114.011359.
 18. Ghanem RN, Jia P, Ramanathan C, Ryu K, Markowitz A, Rudy Y. Noninvasive Electrocardiographic Imaging (ECGI): Comparison to intraoperative mapping in patients. *Heart Rhythm*. 2005;2(4):339-354. doi:10.1016/j.hrthm.2004.12.022.
 19. Donnelly MP, Finlay DD, Nugent CD, Black ND. Lead selection: old and new methods for locating the most electrocardiogram information. *J Electrocardiol*. 2008;41(3):257-263. doi:10.1016/j.jelectrocard.2008.02.004.
 20. Hoekema R, Uijen GJH, van Oosterom A. On Selecting a Body Surface Mapping Procedure. *J Electrocardiol*. 1999;32(2):93-101. doi:10.1016/S0022-0736(99)90088-2.
 21. Cluitmans MJM, Karel J, Bonizzi P, et al. In-vivo Evaluation of Reduced-Lead-Systems in Noninvasive Reconstruction and Localization of Cardiac Electrical Activity. *Comput Cardiol Conf*. 2015. doi:10.1109/CIC.2015.7408626.
 22. Postema PG, van Dessel PFHM, Kors JA, et al. Local Depolarization Abnormalities Are the Dominant Pathophysiologic Mechanism for Type 1 Electrocardiogram in Brugada Syndrome: A Study of Electrocardiograms, Vectorcardiograms, and Body Surface Potential Maps During Ajmaline Provocation. *J Am Coll Cardiol*. 2010;55(8):789-797. doi:10.1016/j.jacc.2009.11.033.
 23. Visser M, van der Heijden JF, Doevendans PA, Loh P, Wilde AA, Hassink RJ. Idiopathic Ventricular Fibrillation: The Struggle of Definition, Diagnosis, and Follow-Up. *Circ Arrhythmia Electrophysiol*. 2016;9(5):e003817. doi:10.1161/CIRCEP.115.003817.
 24. Remme CA, Wever EFD, Wilde AAM, Derksen R, Hauer RNW. Diagnosis and long-term follow-up of the Brugada syndrome in patients with idiopathic ventricular fibrillation. *Eur Heart J*. 2001;22(5):400-409. doi:10.1053/euhj.2000.2366.
 25. Visser M, van der Heijden JF, van der Smagt JJ, et al. Long-Term Outcome of Patients Initially Diagnosed With Idiopathic Ventricular Fibrillation: A Descriptive Study. *Circ Arrhythmia Electrophysiol*. 2016;9(10):e004258. doi:10.1161/CIRCEP.116.004258.
 26. Krahn AD, Healey JS, Chauhan V, et al. Systematic Assessment of Patients with Unexplained Cardiac Arrest: Cardiac Arrest Survivors With Preserved Ejection Fraction Registry (CASPER). *Circulation*. 2009;120(4):278-285. doi:10.1161/CIRCULATIONAHA.109.853143.
 27. Steinberg C, Padfield GJ, Champagne J, et al. Cardiac Abnormalities in First-Degree Relatives of Unexplained Cardiac Arrest Victims: A Report From the Cardiac Arrest Survivors With Preserved Ejection Fraction Registry. *Circ Arrhythmia Electrophysiol*. 2016;9(9). doi:10.1161/CIRCEP.115.004274.
 28. Millar CK, Kralios FA, Lux RL. Correlation between refractory periods and activation-recovery intervals from electrograms: effects of rate and adrenergic interventions. *Circulation*. 1985;72(6):1372-1379. doi:10.1161/01.cir.72.6.1372.
 29. Ramanathan C, Ghanem RN, Jia P, Ryu K, Rudy Y. Noninvasive electrocardiographic imaging for cardiac electrophysiology and arrhythmia. *Nat Med*. 2004;10(4):422-428. doi:10.1038/nm1011.
 30. Ramanathan C, Jia P, Ghanem R, Ryu K, Rudy Y. Activation and repolarization of the normal human heart under complete physiological conditions. *PNAS*. 2006;103(16):6309-6314. doi:10.1073/pnas.0601533103.

31. Conrath CE, Opthof T. Ventricular repolarization: An overview of (patho)physiology, sympathetic effects and genetic aspects. *Prog Biophys Mol Biol*. 2006;92(3):269-307. doi:10.1016/j.pbiomolbio.2005.05.009.
32. Antzelevitch C, Shimizu W, Yan GX, et al. The M cell: its contribution to the ECG and to normal and abnormal electrical function of the heart. *J Cardiovasc Electrophysiol*. 1999;10(8):1124-1152. doi:10.1111/j.1540-8167.1999.tb00287.x.
33. Yan G, Lankipalli RS, Burke JF, Musco S, Kowey PR. Ventricular repolarization components on the electrocardiogram: Cellular basis and clinical significance. *J Am Coll Cardiol*. 2003;42(3):401-409. doi:10.1016/S0735-1097(03)00713-7.
34. Malik M. Ventricular repolarization. *J Electrocardiol*. 2011;44(3):299-300. doi:10.1016/j.jelectrocard.2011.02.004.
35. Monitillo F, Leone M, Rizzo C, Passantino A, Iacoviello M. Ventricular repolarization measures for arrhythmic risk stratification. *World J Cardiol*. 2016;8(1):57-73. doi:10.4330/wjc.v8.i1.57.
36. Castro-Torres Y, Carmona-Puerta R, Katholi RE. Ventricular Repolarization Markers for Predicting Malignant Arrhythmias in Clinical Practice. *World J Clin Cases*. 2015;3(8):705-720. doi:10.12998/wjcc.v3.i8.705.
37. Rudy Y. Noninvasive Electrocardiographic Imaging (ECGI) of Arrhythmogenic Substrates in Humans. *Circ Res*. 2013;112(5):863-874. doi:10.1161/CIRCRESAHA.112.279315.
38. Cluitmans MJM, Clerx M, Vandersickel N, Peeters RLM, Volders PGA, Westra RL. Physiology-based regularization of the electrocardiographic inverse problem. *Med Biol Eng Comput*. 2017;55(8):1353-1365. doi:10.1007/s11517-016-1595-5.
39. Hansen PC, O'Leary DP. The use of the L-curve in the regularization of discrete ill-posed problems. *SIAM J Sci Comput*. 1993;14(6):1487-1503. doi:10.1137/0914086.
40. van Dam PM, Oostendorp TF, Linnenbank AC, van Oosterom A. Non-Invasive Imaging of Cardiac Activation and Recovery. *Ann Biomed Eng*. 2009;37(9):1739-1756. doi:10.1007/s10439-009-9747-5.
41. Oster HS, B. T, Lux RL, Ershler PR, Rudy Y. Noninvasive electrocardiographic imaging: reconstruction of epicardia potentials, electrograms, and isochrones and localization of single and multiple electrocardiac events. *Circulation*. 1997;96(3):1012-1024. doi:10.1161/01.cir.96.3.1012.
42. Cluitmans MJM, Bonizzi P, Karel JMH, et al. In Vivo Validation of Electrocardiographic Imaging. *JACC Clin Electrophysiol*. 2017;3(3):232-242. doi:10.1016/j.jacep.2016.11.012.
43. Oosterhoff P, Meijborg VMF, van Dam PM, et al. Experimental Validation of Noninvasive Epicardial and Endocardial Activation Imaging. *Circ Arrhythmia Electrophysiol*. 2016;9(8):e004104. doi:10.1161/CIRCEP.116.004104.
44. Andrews CM, Srinivasan NT, Rosmini S, et al. The Electrical and Structural Substrate of Arrhythmogenic Right Ventricular Cardiomyopathy Determined Using Noninvasive Electrocardiographic Imaging and Late Gadolinium Magnetic Resonance Imaging. *Circ Arrhythmia Electrophysiol*. 2017;10(7):e005105. doi:10.1161/CIRCEP.116.005105.
45. Burnes JE, Taccardi B, MacLeod RS, Rudy Y. Noninvasive ECG Imaging of Electrophysiologically Abnormal Substrates in Infarcted Hearts: A Model Study. *Circulation*. 2000;101(5):533-540. doi:10.1161/01.CIR.101.5.533.
46. Rudy Y. Noninvasive imaging of cardiac electrophysiology and arrhythmia. *Ann N Y Acad Sci*. 2010;1188(1):214-221. doi:10.1111/j.1749-6632.2009.05103.x.
47. Coronel R, de Bakker JMT, Wilms-Schopman FJG, et al. Monophasic action potentials and activation recovery intervals as measures of ventricular action potential duration: Experimental evidence to resolve some controversies. *Heart Rhythm*. 2006;3(9):1043-1050. doi:10.1016/j.hrthm.2006.05.027.

48. Kara V, Ni H, Alday EAP, Zhang H. ECG Imaging to Detect the Site of Ventricular Ischemia Using Torso Electrodes: A Computational Study. *Front Physiol.* 2019;10(50). doi:10.3389/fphys.2019.00050.
49. Macfarlane PW, van Oosterom A, Pahlm O, Kligfield P, Janse M, Camm J. Body Surface Potential Mapping Techniques. In: *Comprehensive Electrocardiology*. 2nd ed. London: Springer; 2011:1362-1374. doi:10.1007/978-1-84882-046-3.
50. Ramanathan C, Rudy Y. Electrocardiographic imaging: II. Effect of torso inhomogeneities on noninvasive reconstruction of epicardial potentials, electrograms, and isochrones. *J Cardiovasc Electrophysiol.* 2001;12(2):241-252. doi:10.1046/j.1540-8167.2001.00241.x.
51. Stenroos M. The transfer matrix for epicardial potential in a piece-wise homogeneous thorax model: the boundary element formulation. *Phys Med Biol.* 2009;54(18):5443-5455. doi:10.1088/0031-9155/54/18/006.
52. Bear LR, Cheng LK, LeGrice IJ, et al. Forward problem of electrocardiography: is it solved? *Circ Arrhythmia Electrophysiol.* 2015;8(3):677-684. doi:10.1161/CIRCEP.114.001573.
53. Milanic M, Jazbinsek V, MacLeod RS, Brooks DH, Hren R. Assessment of regularization techniques for electrocardiographic imaging. *J Electrocardiol.* 2014;47(1):20-28. doi:10.1016/j.jelectrocard.2013.10.004.
54. Pullan AJ, Cheng LK, Nash MP, Ghodrati A, MacLeod R, Brooks D. The Inverse Problem of Electrocardiography. In: Macfarlane PW, van Oosterom A, Olle P, Paul K, Michiel J, Camm J, eds. *Comprehensive Electrocardiology*. ; 2010:299-344. doi:10.1007/978-1-84882-046-3_9.
55. van Beelen T. EDFbrowser. <https://www.teuniz.net/edfbrowser/>.
56. Tereshchenko LG, Josephson ME. Frequency Content and Characteristics of Ventricular Conduction. *J Electrocardiol.* 2015;48(6):933-937. doi:10.1016/j.jelectrocard.2015.08.034.
57. Gharbalchi No F, Serinagoaglu Dogrusoz Y, Onak ON, Weber G-W. Reduced leadset selection and performance evaluation in the inverse problem of electrocardiography for reconstructing the ventricularly paced electrograms. *J Electrocardiol.* 2020;60:44-53. doi:10.1016/j.jelectrocard.2020.02.017.
58. Akoglu H. User's guide to correlation coefficients. *Turkish J Emerg Med.* 2018;18(3):91-93. doi:10.1016/j.tjem.2018.08.001.
59. Finlay DD, Nugent CD, Donnelly MP, Mccullagh P, Black ND. Optimal Electrocardiographic Lead Systems: Practical Scenarios in Smart Clothing and Wearable Health Systems. *IEEE Trans Inf Technol Biomed.* 2008;12(4):433-441. doi:10.1109/TITB.2007.896882.
60. Bear L, Potse M, Duchateau J, Zenzemi N, Coudiere Y, Dubois R. Accuracy of Lead Removal vs Linear Interpolation in Non-Invasive Electrocardiographic Imaging (ECGI). *Comput Cardiol (2010)*. 2015;42:941-944. doi:10.1109/CIC.2015.7411067.
61. Jiang Y, Qian C, Hanna R, Farina D, Dössel O. Optimization of the Electrode Positions of Multichannel ECG for the Reconstruction of Ischemic Areas by Solving the Inverse Electrocardiographic Problem. *Int J Bioelectromagn.* 2009;11(1):27-37.
62. Bear LR, Bouhamama O, Cluitmans M, et al. Advantages and pitfalls of noninvasive electrocardiographic imaging. *J Electrocardiol.* 2019;57:S15-S20. doi:10.1016/j.jelectrocard.2019.08.007.
63. Stoks J, Nguyen UC, Peeters R, Volders PGA, Cluitmans MJM. *An Open-Source Algorithm for Standardized Bullseye Visualization of High-Resolution Cardiac Ventricular Data: UNISYS.*; 2020.